Neural oscillators

Bard Ermentrout *
Department of Mathematics
University of Pittsburgh
Pittsburgh, PA 15260.

August 9, 2004

1 Introduction

In this review, I will discuss a number of methods than can be used to mathematically analyze the behavior of coupled neural oscillators and networks of such units. This is by no means an exhaustive review and I refer the reader to the comprehensive reviews by Kopell and Ermentrout [39] or Rubin and Terman [55] which cover many more details. I will begin with a discussion of how oscillations arise in neural models. I then discuss the phase resetting curve, an experimental measure, and how this can be used to analyze coupled neural oscillators. A related method using discrete dynamics is applied to pairs of excitatory-inhibitory local networks. I then discuss a variety of general reduction procedures that lead to drastically simplified models suitable for use in large networks. I conclude with a brief discussion of network behavior.

Oscillations are observed throughout the nervous system at all levels from single cell to large networks. Some of the earliest experiments in physiology were aimed at understanding the underlying mechanisms of rhythmicity in nerve axons. Indeed, Hodgkin & Huxley won their Nobel Prize for dissecting the biophysical mechanisms underlying action potential generation in the giant axon of the squid. Oscillations are often associated with simple repetitive motor patterns such as walking, swimming, chewing, breathing, and copulation. Muscles responsible for these actions are controlled by the outputs of neurons whose outputs in turn are controlled by neural circuits in the brain and spinal cord. For this reason, they are called central pattern generators (CPGs). CPGs in the stomatogastric ganglion in the lobster have been well characterized and the exact wiring and neurons responsible for the activity are in some cases completely known [45]. CPGs produce a variety of regular rhythms that control the behavior of the target muscles. Thus, in the case of CPGs the importance of oscillatory behavior is clear and without doubt. Various models based on

*Supported in part by NIMH and NSF

coupled oscillators have been suggested for quadruped locomotion ([6, 56, 14]). Undulatory swimming in the leech [4], the lamprey[13], and other animals is controlled by a series of segmental oscillators [12].

Oscillations in various areas of the brain are also associated with various pathologies. Epilepsy produces massive rhythmic or near rhythmic behavior throughout large areas of the brain. Parkinsonian tremors appear to be a consequence of pathological rhythmic behavior in an area of the brain called the basal ganglia. Large amplitude rhythmic electroencephalographic (EEG) activity is found in patients suffering from Creutzfeldt-Jacob disease. Oscillations occur throughout large regions of the brain during anaesthesia and sleep.

The possible role of oscillatory activity in normal sensory and cognitive behavior is more controversial. It has been suggested that synchronous oscillations in cortex and the phase and timing information they confer could be used to bind together different aspects of a sensory stimulus [31, 57]. Synchronous oscillations in the antennal lobe of insects appear to enhance the ability of the animal to distinguish between two closely related odors [58]. In [25], we suggested that synchronous oscillatory activity enhanced the competition different stimuli thus making it possible to direct attention the the more salient one. In a series of papers [20, 28] we studied the role of oscillations and waves in the learning of odors by the slug by modeling neurons in the procerebral lobe. Ulinski and coworkers [47] have analyzed stimulus-induced waves in the turtle visual area and suggest that the patterns of these waves are characterizing the stimulus in a global distributed fashion. Lam et al [42] suggest that odors are encoded by patterns of oscillations in the turtle olfactory bulb. In spite of the large experimental literature on these sensory-induced oscillations, there is still no definitive evidence for their role in cognition.

2 How does rhythmicity arise

In this section, I discuss the mechanisms that generate periodic behavior from the point of view of nonlinear dynamics. I will only sketch the main points; a thorough and detailed account can be found in [54]. Suppose that we consider a nonlinear differential equation of the form:

$$\frac{dx}{dt} = F(x, \alpha) \tag{1}$$

where α is a parameter and $x \in R^n$. Most models of neurons have a resting state which corresponds to a fixed point of the system (1). As the parameter increases, we assume that a limit cycle arises. There are several mechanisms by which this can happen. The best known is the Hopf bifurcation (HB). In the HB, the fixed point $x_0(\alpha)$ becomes unstable at $\alpha = \alpha_0$ when a complex conjugate pair of eigenvalues of the linearized system cross the imaginary axis at $\pm i\omega$. Generically, a branch of periodic orbits emerges from this fixed point; these cycles have small amplitude and have the form:

$$x(t) = x_0(\alpha_0) + \epsilon z(t) \Phi e^{i\omega t} + cc$$

where "cc" means complex conjugates, Φ is a fixed complex vector depending on the problem and $z(t)$ is a complex scalar which satisfies

$$\frac{dz}{dt} = \epsilon[a(\alpha - \alpha_0)z + cz^2\bar{z}] \tag{2}$$

with a, c complex constants. If $\mathrm{Re}\, c < 0$ we say that the bifurcation is *supercritical* and the resulting branch of small amplitude periodic orbits is stable (Fig 1A). If $\mathrm{Re} c > 0$, then the bifurcation is *subcritical* and the resulting oscillations are unstable. In most neural models, the unstable branches turn around and produce stable periodic orbits which have large amplitude. This is shown in Figure 1B. This case is quite interesting since, for a range of parameters near α_0, there is both a stable fixed point and a stable large amplitude oscillation separated in phase space by the unstable small amplitude periodic orbit. The frequency of oscillations in a Hopf bifurcation is generally confined to a rather limited range (Fig 1D). Hodgkin [34] classified the firing patterns of nerve axons into two different classes : Class I and Class II excitability. (Also called Type I and Type II). In Rinzel and Ermentrout, we suggest that the properties of type II neurons are consistent with the dynamics resulting from a Hopf bifurcation.

A second common way for oscillations to emerge from a fixed point is through a saddle-node infinite-period bifurcation. Unlike the Hopf bifurcation, this is a global bifurcation and requires knowledge of the full phase space in order to prove. Figure 1C illustrates this bifurcation. There is a stable fixed point x_n and a saddlepoint x_s with a one-dimensional unstable manifold and an $n-1-$*dimensional* stable manifold. The branches of the unstable manifold terminate on the stable fixed point forming a heteroclinic loop. As the parameter α changes, these two fixed points merge at a saddle-node bifurcation. However, the global loop still remains (see Figure 1C) and as the parameter passes through α_0, the fixed points disappear leaving a large amplitude stable periodic orbit. The frequency of this orbit can be arbitrarily low and scales as $\sqrt{\alpha - \alpha_0}$ (Fig 1F.) Rinzel and Ermentrout suggest that the properties of class I (Type I) neurons are consistent with this type of dynamics. The local behavior of a saddle-node is captured by the normal form [41]:

$$\frac{dx}{dt} = qx^2 + b(\alpha - \alpha_0) \tag{3}$$

where $q > 0, b > 0$ are problem dependent parameters. When $\alpha > \alpha_0$ (3) has no fixed points and any initial conditions tend to infinity in finite time. The real line can be mapped onto the circle so that this "blow-up" no longer occurs by making the change of variables, $x = \tan\theta/2$ leading to:

$$\frac{d\theta}{dt} = q(1 - \cos\theta) + b(1 + \cos\theta)[\alpha - \alpha_0]. \tag{4}$$

In spite of the global nature of the dynamics, in [22] we show that the behavior near the saddle-node on a circle is captured by this simple scalar model. This model is often used to simulate spiking neurons and is called the "theta" model.

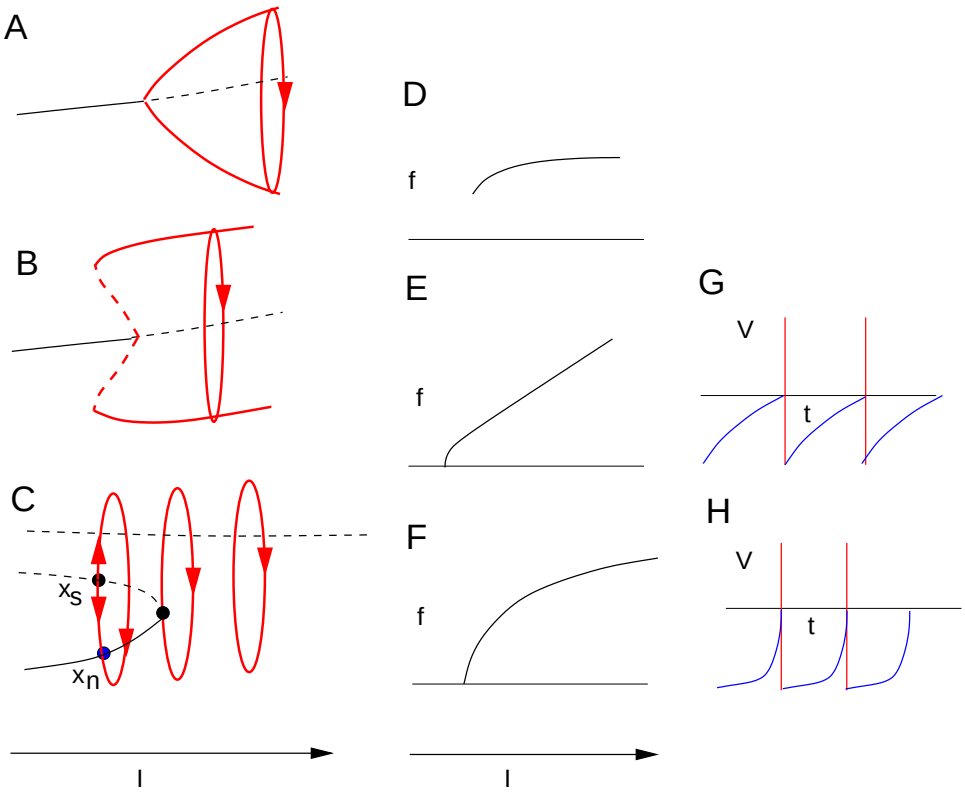

Figure 1: Firing rates for neuron models. (A) Onset of periodicity through a supercritical Hopf bifurcation leading to small amplitude stable periodic orbits (B) Subcritical Hopf bifurcation showing large amplitude limit cycles and bistability between oscillations and the fixed point. (C) Saddle-node on a limit cycle bifurcation to large amplitude periodic orbits. (D) Frequency (firing rate) as a function of current for the bifurcations in A,B. (E) Frequency versus current for the leaky integrate-and-fire model (LIF). (F) Frequency versus current for the bifurcation C and for the quadratic integrate-and-fire model (QIF). (G) Voltage plots for the LIF model with spikes painted on. (H) Voltage plots for the QIF model.

It seems to be a better model for the dynamics of cortical inhibitory neurons than the Hopf bifurcation model. Note that under this change of variables, $\theta = \pi$ is equivalent to approaching $+\infty$ and "resetting" to $-\infty$ in the original equation (3). If, instead of letting x reach $+\infty$ in equation (3)and then resetting to $-\infty$ we reset to a finite value x_{reset} when x crosses x_{spike}, then we obtain a simple computational model for a spiking neuron called the quadratic integrate-and-fire (QIF) model. This was first introduced by Latham et al [43] in the following equivalent form:

$$\tau \frac{dV}{dt} = \frac{(V - V_{rest})(V - V_{thresh})}{V_{thresh} - V_{rest}} + R_m I \tag{5}$$

where I is the applied current, R_m is the membrane resistance of the cell, τ is a characteristic time constant, V_{rest} is the resting state of the neuron, and V_{thresh} is the threshold for excitability. Clearly as I increases, the two fixed points of this model merge at a saddle-node and for I large enough, disappear. The voltage V is reset to a finite value, $V_{reset} > -\infty$ when it reaches a finite value $V_{spike} < \infty$.

A simpler model for spiking neurons but one which cannot be derived from any type of bifurcation is the leaky integrate and fire model (LIF) which has the form:

$$\tau \frac{dV}{dt} = -(V - V_{rest}) + R_m I.$$

The LIF model is reset to V_{reset} whenever V crosses a value V_{spike}. The approach to a spike for the LIF model is concave down while that of the QIF is both. Figure 1E,F shows the output frequency of the LIF and the QIF models to a constant current, I. Note that due to its equivalence, the QIF and the saddle-node model have the same firing rate curve. Figures 1G,H show the shape of the membrane potential, $V(t)$ for several cycles; spikes are painted on whenever the spike-threshold is crossed. The LIF model is often used for analysis since it can be exactly solved even when I varies in time. This is not true for the QIF model and the theta model. (However, for sinusoidal stimuli, the theta model can be transformed into the Mathieu equation, [22]).

We point out one last model related to the QIF that is due to Izhikevich [36] and which can produce many of the spiking patterns of cortical neurons by changing parameters. If we add a simple linear negative feedback term to the QIF, we obtain the following model:

$$\frac{dV}{dt} = (v^2 + 125v)/25 + 140 + I - z \quad \frac{dz}{dt} = a(bv - z)$$

along with the the reset conditions, when $v = +30$ then $v = c$ and $z = z + d$. Here I is the input and a, b, c, d are free parameters. Ermentrout and colleagues [17, 26] also considered this system when $b = 0$ as a model for high-threshold spike frequency adaptation. The additional term, b makes this similar to adding low-threshold adaptation.

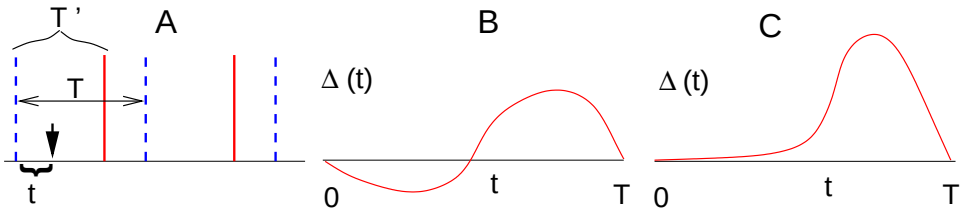

Figure 2: Phase response curves (PRC). (A) Construction of the PRC. Natural period is T. A perturbation arrives at t after the last spike causing the spike to change its time to T'. The PRC, $\Delta(t) = 1 - T'/T$. Dashed pulses show the times at which the oscillator fires without the perturbatioin and the solid curves show the perturbed firing times. Note that a key assumption is that effect of the perturbation occurs only during the cycle it was given. (B) PRC for the firefly *P. Malaccae.* (C) PRC for a cortical neuron.

3 Phase-resetting and coupling through maps.

The stability properties of periodic orbits of autonomous differential equations are different from those of fixed points. There is always a zero eigenvalue which corresponds to translation in time of the orbit. This means that when a limit cycle is perturbed through an external stimulus, there can be a phase shift. This extra degree of freedom is what leads to the ability of several coupled oscillators to maintain differences in timing. It is also what is responsible for jet-lag; the internal circadian oscillator (body clock) needs to be rest by sunlight and this can take several days. Experimentalists have long known about the ability of oscillators to shift their phase and the quantification of this shift is one of the standard methods to characterize a biological oscillator. The basic thesis is that if I know how an oscillator shifts its phase to a stimulus, then I can use this to study entrainment by periodic stimuli and other oscillators. That is, given the *phase-resetting curve* (PRC) for an oscillator, it is possible to construct a map for the behavior when it is periodically driven or coupled to other similar oscillators.

Figure 2A shows how the PRC is constructed. A convenient measure of the timing of a neuron is the time of its action potential, so we assume that the oscillator in question has a well define event corresponding to the start of a cycle. Suppose the period of the unperturbed oscillator is T and a brief stimulus is given at $t \in [0, T)$. This causes the oscillator to shift its timing (that is, the time of the next event) to a time T'. We define the PRC to be

$$\Delta(t) \equiv 1 - \frac{T'}{T}$$

If we define $\phi = t/T$ as the phase of the oscillator, we can define this function in terms of ϕ, $\Delta[\phi] = \Delta(\phi T)$. If $\Delta(t) > 0$ (respectively $\Delta(t) < 0$), this means that the oscillator fired early (late) and the phase was advanced (delayed). Certain species of SE Asian fireflies (notably, *Pteroptx mallacae* or *P. cribellata*)

congregate by the thousands in trees along riverbanks and after some time, flash synchronously with a period of about a second. The the PRC for a single firefly has been measured [33, 5] to understand how such synchronization could take place. Figure 2B shows the form of the PRC for *P. mallacae* which is roughly sinusoidal. We note that the PRC for an oscillator near a Hopf bifurcation has essentially the same shape. Figure 2C shows the PRC form for a cortical neuron injected with constant current (to make it oscillate) and then subjected to brief depolarizing pulses [53]. The main difference between the two PRCs is that the cortical one is basically positive over the whole range of perturbation times. Positive PRCs are characteristic of model neurons which become periodic through a saddle-node bifurcation (Type I). Suppose that we parameterize the PRC by the amplitude of the perturbing stimulus, $\Delta(t,a)$. Then consider

$$Z(t) \equiv \lim_{a\to 0} \frac{\Delta(t,a)}{a}.$$

This is called the infinitesimal PRC. Now suppose the model for the oscillator has the form:

$$\frac{dV}{dt} = F(V, w_1, \ldots, w_n), \quad , \frac{dw_j}{dt} = g_j(V, w_1, \ldots, w_n)$$

and the perturbation is applied only to the equation for V. Let $(V^0(t), w_j^0(t))$ be the limit cycle solution to this equation with the maximum of V occurring at $t = 0$. Then, the infinitesimal PRC, $Z(t)$ is proportional to the V component of the adjoint solution (see [32, 23]). Recall that if $X' = F(X)$ has a periodic solution, $X_0(t)$, then the adjoint, $X^*(t)$ satisfies $X^{*\prime}(t) = -D_X F(X_0(t))^T X^*(t)$ with $X^{*T}(0)X_0'(0) = 1$. This makes the calculation of the PRC for models simple, one need only compute the adjoint to a given periodic solution. This also allows one to explicitly calculate the PRC for certain simple oscillators. The PRC for the theta model, equation (4), is proportional to $(1-\cos(t))$ while that for a supercritical Hopf bifurcation, equation (2), is proportional to $\sin(t)$ where the period of the oscillation is 2π and the spike occurs at $t = 0$. Many PRCs in biology satisfy $\Delta(0) = \Delta(T) = 0$.

Looking at the PRC for the firefly (figure 2B), it is intuitively easy to see how a pair of mutually coupled oscillators could synchronize. Suppose oscillator 1 fires slightly before oscillator 2. Then it will speed up oscillator 2 since the PRC is positive right before the spike. Once oscillator 2 fires, this will slow down oscillator 1 since it has recently fired. Thus, the oscillator ahead is slowed down and the one behind is sped up. We can formalize by creating a model for a pair of mutually coupled oscillators. But before doing this, we first consider an oscillator that is periodically driven by a small pulsatile stimulus with a period P relative to the period of the oscillator. Let ϕ_n be the phase of an oscillator ($\phi \in (0,1]$) at the point the n^{th} stimulus arrives. The phase is incremented by an amount $\Delta(x_n)$ immediately after the stimulus. Then between stimuli, the oscillator advances by an amount P, so that we obtain

$$\phi_{n+1} = \phi_n + \Delta(\phi_n) + P \equiv G(\phi_n; P) \tag{6}$$

We will assume that the stimulus is weak enough so that the function $F(x) = x + \Delta(x)$ is monotone increaing. (This means that $\Delta'(t) > -1$.) We also assume that $\Delta(0) = \Delta(1) = 0$. This implies that the map $F : [0,1) \longrightarrow [0,1)$ is invertible. This has many implications for the forced oscillator; notably that the ratio,

$$\rho = \lim_{n\to\infty} \frac{\phi_n}{n}$$

is almost everywhere rational and a continuous function of the parameters of the model. It is called *rotation number.* On regions where ρ is rational, we say that the oscillator is phaselocked to the stimulus. One solution of interest to (6) is 1:1 locking. This solution requires that $\rho = 1$ and that $\phi_{n+1} = \phi_n + 1$. The latter definition implies that $\phi_n = \bar{\phi}$ satisfies

$$1 - P = \Delta(\bar{\phi}).$$

Since $\Delta(\phi)$ is periodic, solutions are lost in pairs at saddle-node bifurcations. (For example, suppose that $\Delta(\phi) = -a \sin 2\pi\phi$. Then if $|1 - P| > |a|$ there are no fixed points and if $|1 - P| < |a|$ there are two fixed points; a saddle-node occurs at $|1 - P| = |a|$.) For a PRC such as the firefly's, it is possible to obtain 1:1 locking for periods, P both shorter and longer than the natural period of the oscillator. However, for oscillators with a PRC like type I oscillators or like the cortical neuron, it is only possible to lock to stimuli that are faster than the intrinsic period, *i.e.*, $P < 1$. This is intuitively obvious; stimuli can only speed up the oscillator since the PRC is positive. A 1:1 locked solution is stable if and only if

$$|F'(\bar{\phi})| = |1 + \Delta'(\bar{\phi})| < 1.$$

By hypothesis, $\Delta'(\phi) > -1$ so that the necessary condition for stability is that $\Delta'(\bar{\phi}) < 0$. For the PRCs illustrated above, the solution stable solution occurs on the falling side of the PRC.

We now turn to the analysis of the behavior of a pair of identical reciprocally coupled oscillators ([30]). We suppose that the period of each is 1 without loss in generality. We will write the coupled system, formally, as a set of differential equations and from this derive a locally defined map near a particular periodic solution:

$$\dot{\theta}_1 = 1 + \delta(\theta_2)\Delta(\theta_1), \quad \dot{\theta}_2 = 1 + \delta(\theta_1)\Delta(\theta_2). \tag{7}$$

Each time, say, oscillator 1 fires (that is, crosses 0 modulo 1), then oscillator 2 has its phase altered as $\theta_2 = \theta_2 + \Delta(\theta_2) \equiv F(\theta_2)$. The function, $F(\theta)$ is called the phase-transition curve. Note that our assumptions on $\Delta(\theta)$, namely that $\Delta'(\theta) > -1$, and that $\Delta(0) = \Delta(1) = 0$ imply that $F(\theta)$ is monotone, with $F(0) = 0$ and $F(1) = 1$. Suppose that θ_1 fires a spike at $t = 0$ and $\theta_2 = \phi$. Then immediately after the spike, $\theta_2 = F(\phi) < 1$ since F is monotone and $F(1) = 1$. θ_2 will spike at $t_2 = 1 - F(\phi)$ at which point θ_1 has advanced by an amount t_2. The spike elicited by θ_2 advances θ_1 to $F(1 - F(\phi))$ while θ_2 is set to 0. θ_1 will next fire at $t_1 = 1 - F(1 - F(\phi))$ and θ_2 has advanced by the same amount. Thus, we have the map

$$\phi \longrightarrow 1 - F(1 - F(\phi)) \equiv Q(\phi).$$

Note that $Q(0) = 0$ so that $\phi = 0$ is always a fixed point of the map. Other fixed points are found by solving $\phi = Q(\phi)$. The fixed point, $\bar{\phi}$ is stable if $|Q'(\bar{\phi})| < 1$ which translates to $F'(1 - F(\bar{\phi})) \cdot F'(\bar{\phi}) < 1$ since $F'(\phi) > 0$. This is the product of two terms; the derivative of the phase-transition curve evaluated at the phase of each oscillator when the other fires a spike. In particular, consider the synchronous solution. This will be stable if $F'(1^-)F'(0^+) < 1$ or, $[1 + \Delta'(1^-)][1 + \Delta'(0^+)] < 1$. Consider the firefly PRC. Then since $\Delta'(0^+) < 0$ and $\Delta'(1^-) < 0$, this means that synchrony is always stable. On the other hand, it is not necessary that the derivative of Δ is continuous at 0, so that it may be that case that $\Delta'(1^-) = \Delta'(0^-) \neq \Delta'(0^+)$. This appears to be the case for cortical PRCs for which $\Delta'(0^+) > 0$ and $\Delta'(1^-) < 0$. For the PRC shown in figure 2C, for example, since the slope at 0 is positive but shallow and the slope at 1 is steep and negative, this implies that $Q'(0) < 1$ so that synchrony is stable.

We can use these general methods to create networks of coupled cells through their PRCs:

$$\dot{\theta}_j = \omega_j + \sum_k \delta(\theta_k)\Delta_{jk}(\theta_j),$$

where we allow for some slight differences in natural frequencies, ω_j. In [30], we consider rings of cells for which we prove the existence and stability of traveling waves. We also consider two-dimensional arrays of cells with nearest neighbor interactions. We show the existence of rotating waves in such a network.

We close this section with a simplification of the general pulse-coupled network:

$$\frac{d\theta_j}{dt} = \omega + \sum_k g_{jk} P(\theta_k)\Delta(\theta_j). \tag{8}$$

In this model, the Dirac function is replaced by a smooth pulse function and all cells have the same PRC; the only difference lies in the coupling amplitudes, g_{jk}. This model was suggested by Winfree [64]. Suppose that $g_{jk} \geq 0$ and that $G = \sum_k g_{jk}$ is independent of j. Let

$$\frac{d\theta}{dt} = \omega + GP(\theta)\Delta(\theta)$$

have a solution $\theta(t) = \phi(t)$ with $\phi'(t) > 0$ and $\phi(0) = 0, \phi(T) = 1$ for some $T > 0$. Then (i) there is a synchronous solution to (8), $\theta_j(t) = \phi(t)$ and (ii) it is asymptotically stable if

$$\int_0^T P(\phi(t))\Delta'(\phi(t))\ dt < 0.$$

We remark that this depends crucially on the non-negativity of g_{jk}. We also note that if $\Delta(\theta)$ is similar to the firefly in that it is decreasing around the origin and $P(\theta)$ is sharply peaked around the origin, nonnegative, and vanishes outside some small neighborhood of the origin, then the stability condition will hold.

4 Doublets, delays, and more maps

In [24] we used maps to explain the importance of inhibitory doublets for synchronizing two distant populations of neurons that were producing a so-called gamma rhythm of about 40 Hz. Each population consists of excitatory and inhibitory neurons which are locally coupled in such a way that they are synchronous within the population. In the local populations, there are few (or weak) excitatory-excitatory connections. Between distant groups, the excitatory cells of one group connect to the inhibitory cells of the other group and because the groups are far apart, the connection between them has a delay. In large scale simulations of this setup [59, 60], thye found that the inhibitory population of cells fires a pair of spikes (called a doublet) when the two populations of excitatory cells were synchronized. Our approach to this problem was to consider a firing time map for the spike times of the excitatory population. The basic ideas are as follows. E cells cannot fire until the inhibition from them has worn off below a certain level. Each time an I cell fires the synapse to the E cell is set to its maximum conductance and then it decays exponentially. When an I cell receives excitation, it fires a spike at a time that depends on the last time that it spiked. In particular, if the I cell has recently spiked, then an incoming E spike may not cause the I cell to spike (absolute refractoriness) or if it does spike, it is with some perhaps lengthy delay. Indeed, because the I cell models are class I excitable, they can fire with an arbitrarily long latency if the stimulus is timed right. We now derive a simple map for the synchronization of these two groups of oscillators. The key feature that is responsible for the synchronization of the pair is the recovery map for the inhibitory neurons, $T_I(t)$. Specifically, $T_I(t)$ is the time that the I cell fires its next spike given that it has received an E spike t milliseconds since it last fired. This map can be computed numerically by firing an E cell at different times after the I cells has spiked and measuring the latency to the next spike. For t large, the map approaches a small positive latency, T_{ei}. For t small, the map is rather steep and in fact, it may be undefined for t small enough. Recurrent inhibitory synapses make the map steeper since they act to make the I cell even more refractory. Stronger excitatory inputs make the map shallower and lower the latency for all times. The map can be approximated by the function:

$$T_I(t) = T_{ei} + \frac{a}{t+b}.$$

If $b < 0$, then the map is undefined for $t < -b$.

A brief digression Allow me to digress briefly and derive this map from the biophysics of the I cell. The I cell is a type I neuron so that at the bifurcation, the dynamics is approximated by $dx/dt = qx^2$ (see equation (3). Suppose that the impulse from the E cell arrives at t^* and $x(0) = -x_0$ is the degree of refractoriness of the I cell right after firing. Until the I cell receives input,

$$x(t) = \frac{-1}{1/x_0 + qt}$$

and when the input comes

$$x(t^{*+}) = A - \frac{1}{1/x_0 + qt^*}$$

where A is the amplitude of the input. Firing is defined as when the solution "blows up" which occurs when

$$\begin{aligned} t_{fire} &\equiv \frac{q}{A - \frac{1}{1/x_0 + qt^*}} \\ &= T_{ei} + \frac{a}{t^* + b} \end{aligned}$$

where

$$T_{ei} = \frac{q}{A}, \quad a = A^{-2}, \quad \text{and } b = \frac{1}{q}\left(\frac{1}{x_0} - \frac{1}{A}\right).$$

With this little derivation, we can assign meaning to each of the parameters. The larger the refractory period, x_0, the more negative the parameter b. Similarly, the larger the value of the excitatory stimulus, the shallower the map. For sufficiently large stimulus, the map is defined for $t = 0$, i.e., $T_I(\theta) > 0$.

End of digression

We assume that there is a conduction delay, δ, of the impulse from an E cell in one group to the I cell in the other group. We are interested in the ability of the two groups to synchronize stably in the presence of this delay. We suppose that an E cell fires a fixed amount of time T_{ie} after the last I spike that it has received in a cycle. This is not unreasonable given our assumption that the I cell synapses always produce their maximal conductance when the I cells spike. This also implicitly assumes that the E cells have no slow processes that are turned on when the E cell spikes. (For example, strong spike-frequency adaptation would make the present analysis suspect. Indeed in [40] we include adaptation in the excitatory cells and show that the behavior is quite different. In [24], we in fact incorporate some memory of the previous spikes for the E cells, but to keep matters simple, we ignore it here.) Let t_j be the time of firing of the excitatory neuron in group j ($j = 1, 2$) at the start of a cycle. By this time the I cells in that group are completely recovered so that they fire at a time, $t_j + T_{ei}$. The I cell in group 1 receives an extrinsic E spike at time $t_2 + \delta$, so that this I cell will fire another spike (the "doublet") at a time,

$$t_1^{doub} = t_2 + \delta + T_I[t_2 + \delta - (t_1 + T_{ei})]$$

The E cell in group 1 will then fire its next spike at $t_1^{new} = t_1^{doub} + T_{ie}$. This leads to the following map:

$$\begin{aligned} t_1^{new} &= t_2 + \delta + T_I(t_2 - t_1 + \delta - T_{ei}) + T_{ie} \\ t_2^{new} &= t_1 + \delta + T_I(t_1 - t_2 + \delta - T_{ei}) + T_{ie}. \end{aligned}$$

We let ϕ be the timing difference between the two groups, $\phi = t_2 - t_2$ so that ϕ satisfies

$$\phi^{new} = -\phi + T_I(-\phi + \delta - T_{ei}) - T_I(\phi + \delta - T_{ei}) \equiv G(\phi). \tag{9}$$

Clearly, $G(0) = 0$ so that synchrony (0 time difference) is a solution. Our interest is in its stability. This requires that $|G'(0)| < 1$ or $|-1-2T_I'(\delta - T_{ei})| < 1$ which simplifies to $T_I'(\delta - T_{ei}) > -1$ since T_I' is always negative. Applying this to our approximate map, we see that we must have

$$\delta > a - b + T_{ei} = A^2 + \frac{q}{A} + \frac{1}{q}\left(\frac{1}{A} - \frac{1}{x_0}\right).$$

However, for large values of δ, T_I' is nearly zero so that $G'(0)$ is close to -1 so that small heterogeneities in the two networks (say, T_{ie} is different from one to the other) will lead to an inability to lock, not through stability, but through existence. That is, if, for example, the two oscillators have different values of T_{ie}, then equation (9) is replaced by

$$\phi^{new} = G(\phi) - B$$

where B is the difference between the values of T_{ie}. Fixed points satisfy:

$$T_I(-\phi + \delta - T_{ei}) - T_I(\phi + \delta - T_{ei}) = B.$$

For large δ the left-hand side is nearly zero so that if B, the heterogeneity, is too large, there are no fixed points.

The maps derived in this section allow us to make some general conclusions about the roles of different parameters. First, if the delay is too small, then the slope of the T_I map is large and negative so that we expect to see instabilities. Increasing the $I-I$ coupling makes the map steeper since it essentially makes the I cells more refractory. The steeper the T_I map, the more difficult it is to stably lock for short delays. On the other hand, a steep T_I map is better able to overcome intrinsic differences between the two networks at long delays. Conversely, increasing the $E-I$ coupling makes the network less susceptible to instabilities for short delays but less able to compensate for heterogeneity.

5 Averaging and phase models.

One of the assumptions implicit in the use of phase-resetting curves is that the coupling is not too strong. We can be more explicit about this "weak" coupling assumption by applying averaging to coupled oscillators. Consider the following coupled system in $R^n \times R^n$

$$X_1' = F(X_1) + \epsilon G_1(X_2, X_1), \quad X_2' = F(X_2) + \epsilon G_2(X_2, X_1). \tag{10}$$

We assume that when $\epsilon = 0$, the system $X' = F(X)$ has a phase-asymptotically stable limit cycle solution, $X_0(t)$ with period, T. The limit cycle is homeomorphic to the circle, S^1. Stability means that there is an open neighborhood, N of S^1 in R^n such that all point in N are attracted to the limit cycle. Thus, when $\epsilon = 0$, there is an attracting two-torus, $S^1 \times S^1$ and all points

$(X_1, X_2) \in N \times N$ are attracted to the torus. Each point on the stable limit cycle can be parametrized by a single variable, θ, so that when $\epsilon = 0$, the dynamics on the torus have the form

$$\theta_1' = 1 \qquad \text{and } \theta_2' = 1.$$

The solutions to these uncoupled equations are $\theta_j = t + \phi_j$ where ϕ_j are arbitrary constants. That is, without coupling, the solutions can have arbitrary phases as they move around the torus. For $\epsilon \neq 0$ and sufficiently small we expect that the torus will persist, but that the parallel flow on the torus will collapse toward a phaselocked solution where the difference, $\theta_2 - \theta_1$ takes on isolated values. Indeed, we expect that for nonzero ϵ the equations have the form $\theta_j' = 1 + \epsilon h_j(\theta_j, \theta_k)$. Our goal in this section is to discern the form fo h_j.

In order to derive the equations for $\epsilon > 0$, we introduce some notation. Let B denote the space in R^n of continuous $T-$periodic solutions. We introduce the inner product

$$< u(t), v(t) >= \frac{1}{T} \int_0^T u(t) \cdot v(t)\ dt.$$

$X_0(t)$ is the asymptotically stable limit cycle solution satisfying

$$X_0'(t) = F(X_0(t))$$

so that differentiating this, we see that the linear operator

$$(LY)(t) \equiv -\frac{dY(t)}{dt} + D_X F(X_0(t))Y(t) \equiv [-\frac{d}{dt} + A(t)]Y(t)$$

has a one-dimensional nullspace spanned by $\frac{dX_0(t)}{dt}$. Under the above inner-product, the adjoint operator is

$$(L^* Z)(t) = [\frac{d}{dt} + A^T(t)]Z(t)$$

and this has a one-dimensional nullspace spanned by $Z^*(t)$ which can be normalized to satisfy $Z^*(t) \cdot X_0'(t) = 1$. (For asymptotically stable limit cycles, we can numerically compute $Z^*(t)$ by integrating $(L^* u)(t)$ backwards in time until convergence to a periodic solution is obtained.) Recall from section 3 that $Z^*(t)$ is related to the infinitesimal phase-response curve (see also below). Using the method of averaging [23] it is easy to derive the equations for the evolution of phases, $X_j(t) = X_0(\theta_j) + O(\epsilon)$ where

$$\theta_1' = 1 + \epsilon H_1(\theta_2 - \theta_1) + O(\epsilon^2) \quad \text{ and } \quad \theta_2' = 1 + \epsilon H_2(\theta_1 - \theta_2) + O(\epsilon^2)$$

with

$$H_j(\phi) = \frac{1}{T} \int_0^T Z^*(t) \cdot G_j(X_0(t + \phi), X_0(t))\ dt.$$

Before turning to the analysis of this equation, we apply the formalism to coupled neurons. Single compartment models are generally coupled through the potentials, $V(t)$. Suppose the equations for the voltage have the form:

$$\frac{dV_j}{dt} = \frac{1}{C}\left(-I^j_{ion}(t) + I^{jk}_{syn}(t)\right),$$

where $I^j_{ion}(t)$ are all the ionic currents intrinsic to the cell and $I^{jk}_{syn}(t)$ has the form

$$I^{jk}_{syn}(t) = g^{jk}_{syn} s_k(t)(V_j(t) - E^{jk}_{syn}) + g^{jk}_{gap}(V_j(t) - V_k(t)).$$

The variable $s_k(t)$ is gating variable just like the usual voltage-gated ion channels, but it is gated by the presynaptic voltage, V_k rather than the postsynaptic voltage. The second coupling term is called electrical coupling and depends on the voltage difference between the pre- and post-synaptic cells. Let $V^*(t)$ be the voltage component of the adjoint, $Z^*(t)$; recall that this is proportional to the PRC for the neuron, at least to lowest order. Then

$$H_j(\phi) = \frac{1}{C}\frac{1}{T}\int_0^T V^*(t)\left(g^{jk}_{syn} s_0(t+\phi)(E^{jk}_{syn} - V_0(t)) + g^{jk}_{gap}(V_0(t+\phi) - V_0(t))\right)\, dt.$$

Here $V_0(t), s_0(t)$ are the solutions to the uncoupled system on the limit cycle. Typically, $s_0(t)$ is qualitatively like, $a^2 t e^{-at}$ where t is the time since the neuron spiked during the cycle. Consider the first term in the integral:

$$\frac{1}{C}\frac{1}{T}\int_0^T V^*(t)(E^{jk}_{syn} - V_0(t)) s_0(t+\phi)\, dt \equiv H^{jk}_c(\phi)$$

The terms multiplying s_0 depend only on the postsynaptic cell (the one receiving the synapse). This term characterizes the response of a neuron to the synapse. Thus the first term in the integral is the average of the response with a phase-shift of the input. Note that in general, $H_c(0) \neq 0$. The second term in the integral is

$$\frac{1}{C}\frac{1}{T}\int_0^T Z^*(t)(V_0(t+\phi) - V_0(t))\, dt \equiv H_g(\phi). \tag{11}$$

Note that $H_g(0) = 0$. We make one more observation. Suppose that the coupling from one oscillator to the other is delayed by an amount, say, τ. Then the only effect on the interaction function H is to shift the argument by τ. Intuitively, this is because θ is essentially a time variable so that delays are just translations in time.

Suppose that the two oscillators are coupled identically. Then we can write

$$\theta_1' = 1 + \epsilon H(\theta_2 - \theta_1), \quad \theta_2' = 1 + \epsilon H(\theta_1 - \theta_2),$$

where

$$\begin{aligned} H(\phi) &= g_{gap} H_g(\phi) + g_{syn} H_c(\phi) \\ H_g(\phi) &= \frac{1}{CT}\int_0^T Z^*(t)(V_0(t+\phi) - V_0(t))\, dt, \\ H_c(\phi) &= \frac{1}{CT}\int_0^T Z^*(t) s_0(t+\phi)(E - V_0(t))\, dt. \end{aligned}$$

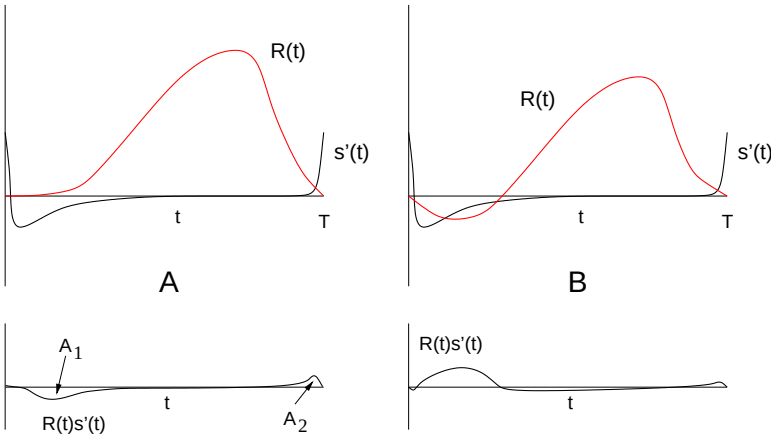

Figure 3: Computation of the stability of synchrony. (A) the derivative of the synapse, $s_0'(t)$ and the response function, $R(t)$. The integral of their product is $H'(0)$ and is negative. (B) If $R(t)$ has a negative region after the spike, the area is positive and synchrony is stable.

Let $\phi = \theta - 2 - \theta_1$. Then

$$\phi' = \epsilon H(-\phi) - H(\phi).$$

The right-hand side is a continuous odd-periodic function so that it has at least two roots, $\phi = 0$ and $\phi = T/2$. The former represents the synchronous solution. It is a stable solution if and only if $-2H'(0) < 0$ which means that $H'(0) > 0$. For chemical synapses,

$$H'(0) = \frac{1}{T}\int_0^T R(t)s_0'(t)\ dt,$$

where $R(t) = Z^*(t)(E - V_0(t))$. Consider first excitatory coupling. For cortical neurons, $R(t)$ has the shape shown in figure 2C. Figure 3 shows $s_0'(t)$, $R(t)$ and their product. From this figure it is also clear that the area of the product $R(t)s_0'(t)$ is negative so synchrony is unstable. Less clear, but shown in specific examples is the fact that the anti-phase solution, $\phi = T/2$ is stable for excitatory coupling. For a PRC like that of the firefly which has a substantial negative region right after the spike (see figure 2B), synchrony is stable as seen in Figure 3B. Since inhibitory coupling essentially reverses the sign of $E - V_0(t)$, synchrony is stable and the anti-phase state is unstable [61, 29, 11, 63]. The behavior of gap junctions is more subtle and depends strongly on the actual shape of the action potential [10]; from the above formula:

$$H_g'(0) = \frac{1}{CT}\int_0^T Z^*(t)V_0'(t)\ dt.$$

Suppose that $Z^*(t)$ is positive and essentially zero and the action potential is short-lasting. Then $V_0'(t)$ is negative only at the beginning of the cycle where $Z^*(t)$ is small. For the majority of the cycle, $V_0'(t) > 0$ as the neuron repolarizes, so that the area under the integral is positive. Thus, we expect that for thin action potentials, synchrony is stable. However, as the frequency of the neuron increases, the action potential occupies a greater portion of the cycle and it may be possible to destabilize synchrony. These simple intuitive arguments are no replacement for the actual calculations. However, they serve to shed insight into how different forms of coupling alter the locked states and how these states depend on frequency.

5.1 Local arrays

So far, we have considered pairs of oscillators and their phaselocked behavior. I will next consider one-dimensional geometries and then use results from this to look at planar arrays of oscillators. Since rings are easier to deal with (there are no boundary effects), we start with them and illustrate traveling waves and synchrony. We then turn our attention to linear arrays in which the edge conditions play a pivotal role it determining the steady state patterns.

The ideas discussed above can be extended in an obvious fashion to large networks of weakly coupled nearly identical cells. This leads to equations of the form:

$$\theta_j' = \omega_j + H_j(\theta_1 - \theta_j, \ldots, \theta_N - \theta_j),\ j = 1, \ldots, N. \tag{12}$$

A *phaselocked state* is one for which $\theta_j(t) = \Omega t + \phi_j$ where $\phi_1 = 0$ and the remaining ϕ_j are constants. Suppose that there is such a state and let

$$a_{jk} = \left.\frac{\partial H_j(\psi_i, \ldots, \psi_N)}{\partial \psi_k}\right|_{\phi_1 - \phi_j, \ldots, \phi_N - \phi_j}.$$

With these preliminaries, we can now state a very general stability theorem.

Theorem 1. [16] *Suppose that $a_{jk} \geq 0$ and the matrix $A = (a_{jk})$ is irreducible. Then the phaselocked state is asymptotically stable.*

This provides a quick sufficient check for stability. If we regard the oscillators as nodes and draw directed line segments from j to k if $a_{jk} > 0$, then irreducibility of the matrix A says that we can go from any given node i to any other node, ℓ by following these directed segments. We also note that stability implies that there are no zero eigenvalues of A other than the simple one corresponding to the translation invariance of limit cycles. Thus, the theorem also provides conditions under which we can continue solutions using the implicit function theorem as some parameter varies. We will apply some of these principles below.

5.1.1 Rings.

Since a general ring of oscillators (even phase models) is impossible to completely analyze, we will assume translation invariance in the model system. That is, we

assume the coupling between oscillators depends only on the differences between their indices. Furthermore, we assume the nature of the coupling between any two oscillators is the same and only the coefficient varies. Thus, we restrict our attention to the system

$$\theta_j' = \omega + \sum_{k=1}^{N} C(j-k)H(\theta_j - \theta_k) \tag{13}$$

where as usual, H is a sufficiently differentiable $2\pi-$periodic function. Equation (13) admits a family of traveling wave solutions of the form

$$\theta_j = \Omega_m t + 2\pi jm/M, \quad m = 0, \ldots N-1.$$

Substitution of this form into (13) implies that

$$\Omega_m = \omega + \sum_k C(k)H(2\pi km/N).$$

This provides the so-called dispersion relation for the waves; that is, how the frequency depends on the wave number, m. Stability of these wave is readily found by linearizing about the solution. The linearized system satisfies

$$y_j' = \sum_k C(j-k)H'(2\pi(j-k)m/N)(y_j - y_k).$$

Because the resulting linearization matrix is circulant, the eigenvectors are of the form $\exp(2\pi ij\ell/N)$ so that for a given m, we have the N eigenvalues

$$\lambda_{\ell,m} = \sum_k C(k)H'(2\pi km/N)(1 - \exp(-2\pi ik\ell/N)).$$

In particular, the synchronous solution has $m = 0$ and the eigenvalues are

$$\lambda_{\ell,0} = H'(0)\sum_k C(k)(1 - \exp(-2\pi ik\ell/N)).$$

If $H'(0) < 0$ and $C(k) \geq 0$, then it follows from Theorem 1 that synchrony is stable. However, if C changes sign, then synchrony is often unstable as are waves with a high value of m, but for some range of values of m, there are stable waves. As an example, consider a network of 100 oscillators with coupling between the 10 neighbors on either side, $C(j) = 1/9$ for $|j| < 5$ and $C(j) = -1/12$ for $10 \geq |j| \geq 5$. The function $H(x) = 0.5\cos x - \sin x$. Then, synchrony is unstable, but the wave with $m = 4$ is stable. Random initial data for this ring network tend to a solution which is a mix of waves propagating in both directions.

5.1.2 Linear arrays

Linear arrays of oscillators, even with only nearest neighbor coupling, are considerably more difficult to analyze. Unless the boundary conditions are chosen very specially, the general behavior is nontrivial. However, with sufficiently long chains, it turns out that the behavior is captured by the solutions to a certain two-point singularly perturbed boundary value problem. Consider the following network:

$$\theta_j' = \omega_j + H_f(\theta_{j+1} - \theta_j) + H_b(\theta_{j-1} - \theta_j), \quad j = 1, \ldots, N, \tag{14}$$

where at $j = 1$ ($j = N$) we drop the H_b (H_f) term. In [37, 38], we showed that the phaselocked behavior of this system satisfies

$$\theta_{j+1} - \theta_j \longrightarrow \Phi(j/N)$$

where

$$\begin{aligned}
\Omega &= \omega(x) + H_f(\Phi) + H_b(-\Phi) + \frac{1}{N}[H_f'(\Phi) - H_b'(-\Phi)]\Phi_x \quad 0 < x < 1 \\
\Omega &= \omega(0) + H_f(\Phi(0)) \\
\Omega &= \omega(1) + H_b(-\Phi(1)).
\end{aligned}$$

For large N, this is a singularly perturbed first order differential equation. As with many singularly perturbed systems, there are boundary layers. In these papers, we exhaustively classify all possible phaselocked solutions for N large by studying the singular boundary value problem and through the use of matching of inner and outer equations. In figure 4, we illustrate various solutions to equation (14) for $N = 80$. Note that for the isotropic case (panel E), the boundary layer is in the interior. Note also, the value of N for which the continuum approximation is reasonable, depends on the parameters of the model. For example, panel F shows little evidence of a boundary layer although one is predicted at both sides for N large enough.

As another example of the behavior of one-dimensional chains, we consider the completely isotropic case with nearest neighnbors in which $H_f(\phi) = H_b(\phi) = H(\phi)$. For large N, the boundary layer (if it exists) will be interior. Suppose that $H(\phi) = C + g(\phi)$ where g is an odd periodic function like $\sin\phi$. Then, $\Phi(x) \approx K(x - 1/2)$ so that, the gradient is linear. In the second example, $H(\phi) = g(\phi + C)$ where, again, g is an odd periodic function. In this case, if g is similar to sin and $|C| < \pi/4$, then $\Phi(x) \approx A\text{sign}(x - 1/2)$. In both of these examples, the phase difference switches signs in the middle so that physically, one observes either waves propagating from the ends toward the middle or vice versa. These examples will play a role shortly.

5.1.3 Frequency plateaus.

In [21], we considered the behavior of a chain of oscillators with a linear frequency gradient. The motivation for this comes from experiments on waves in

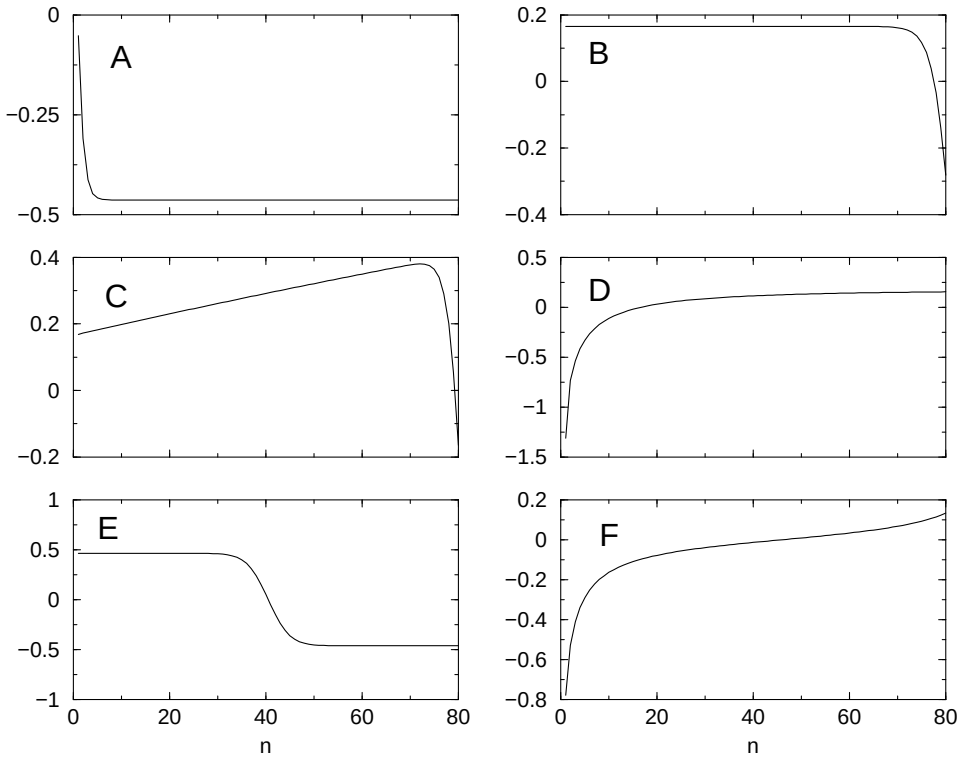

Figure 4: Local phase differences in a chain of 80 nearest-neighbor oscillators under a variety of cases. (A,B,D,F) anisotropic coupling; (C) isotropic coupling with a linear gradient in frequency; (E) isotropic coupling.

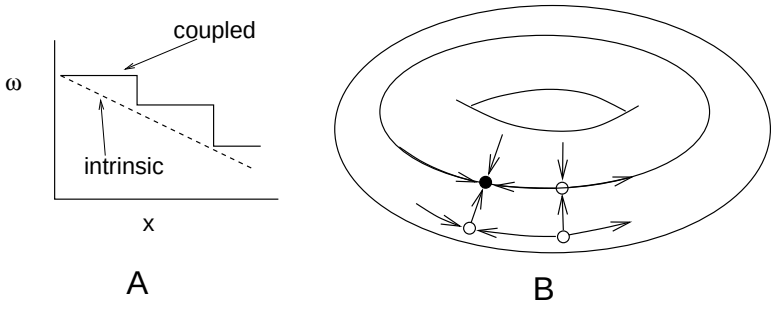

Figure 5: Frequency plateaus in coupled oscillators. Left panel shows the intrinsic linear gradient in frequency and the coupled frequencies. Right panel gives a geometric picture of how plateaus are formed.

the small bowel. Smooth muscle in the bowel generates rhythmic oscillations. A plot of the frequency as a function of distance from the stomach (towards the large bowel) shows that over large regions, the frequency is constant, but, there are abrupt jumps to lower frequencies. When small pieces of the bowel are isolated, they show a linear gradient in natrural frequencies. Figure 5 shows an schematic of the frequency of the intrinsic and the coupled oscillators. We were motivated to study the behavior of a chain of locally coupled oscillators with a linear gradient in frequency:

$$\theta_j' = \omega - gj + H(\theta_{j+1} - \theta_j) + H(\theta_{j-1} - \theta_j) \quad j = 1, \ldots, N+1.$$

Since coupling in the bowel is through gap junctions, $H(0) = 0$. (See equation (11). Suppose, in addition, that $H'(0) > 0$. Then, for $g = 0$, $\theta_j = \Omega t + C$ is a solution. From Theorem 1, it is a stable solution and so we can continue the phaselocked state for g small. As g increases (that is, the frequency gradient increases), phaselocking can become disrupted. Thus, we can ask what happens for large g. This question can be answered to some satisfaction if we make the simplification that the function $H(\theta)$ is odd. For then, we can explicitly write down the solutions for the phase differences, $\phi_j = \theta_{j+1} - \theta_j$:

$$H(\phi_j) = -g\frac{(N-j)j}{2}. \tag{15}$$

Since H is continuous and periodic, it is bounded; thus, there are phaselocked solutions only if g is sufficiently small. Since $H(x) = b$ generically has two roots, x, there are 2^N roots. We show that only one of these is asymptotically stable. Furthermore, we show that there is another fixed point with one positive eigenvalue and all other eigenvalues negative. The two branches of the one-dimensional unstable manifold form a closed invariant circle containing the stable fixed point. Figure 5B shows four fixed points on an invariant torus for $N = 2$. The filled fixed point is stable and the fixed point to the left of it has a one-dimensional unstable manifold forming the circle. Now, suppose that H has

± 1 as it extreme values. Then, from equation (15) $g < g^* \equiv N^2/8$ in order for phaselocking to occur. The righthand hand side is largest in magnitude when $j = N/2$. Thus, as g increases beyond g^*, there is a saddle-node bifurcation. We showed in [21] that the two fixed points on the aforementioned invariant circle merge and leave in their wake, an invariant circle. The frequency of this oscillations is roughly $q = a\sqrt{g - g^*}$ so that the phases, ϕ_j split into two groups. The frequency of the group with $j \leq N/2$ is higher than the group with $j > N/2$ by an amount q, thus the ideas provide a mechanism for frequency plateaus.

5.1.4 Two-dimensions.

The behavior of two-dimensional arrays, with coupling to only four the eight nearest neighbors turns out to be very similar to a cross product of behavior of two associated one-dimensional chains. Thus, in a sense, the equations are like separable PDEs. For simplicity, consider the network:

$$\theta'_{j,k} = \omega + H_N(\theta_{j,k+1} - \theta_{j,k}) + H_S(\theta_{j,k-1} - \theta_{j,k}) + H_E(\theta_{j+1,k} - \theta_{j,k}) + H_W(\theta_{j-1,k} - \theta_{j,k}). \tag{16}$$

There are four different functions corrsponding to the four nearest neighbors. in [52], we analyzed this and generalizations for $N \times N$ arrays where N is large. We showed that

$$\begin{aligned} \theta_{j+1,k} - \theta_{j,k} &\sim \Phi(j/N) \\ \theta_{j,k+1} - \theta_{j,k} &\sim \Psi(j/N) \end{aligned}$$

where $\Phi(x), \Psi(x)$ solved the corresponding horizontal and vertical chains. Thus, in a continuum approximation ($x = j/N, y = k/N$), $\theta_x = \Phi(x)$ and $\theta_y = \Psi(y)$ so that we can integrate this to obtain the full solution:

$$\theta(x, y) = \Omega t + \int_0^x \Phi(x')\ dx' + \int_0^y \Psi(y')\ dy'.$$

In particular, suppose that the medium is completely isotropic and $H_{N,S,E,W}(\phi) = H(\phi)$. Suppose that $H(\phi) = g(\phi) + C$ as in the end of section 5.1.2. Then we know that the phase gradient is linear so that we have:

$$\theta(x, y) = \Omega t + K[(x - \frac{1}{2})^2 + (y - \frac{1}{2})^2].$$

This representa a target wave; curves of constant phase are circles! In the other example from section 5.1.2, $H(\phi) = g(\phi + C)$, we have

$$\theta(x, y) = \Omega t + K[|x - \frac{1}{2}| + |y - \frac{1}{2}|],$$

and waves are "square" target patterns. These and other patterns which are consequences of the theorem in [52] are illustrated in figure 6.

Spiral waves. The two-dimensional patterns described in the previous section are homotopic to the synchronous phaselocked solution and are a consequence of boundary inhomogeneities. Do there exist patterns of phases which

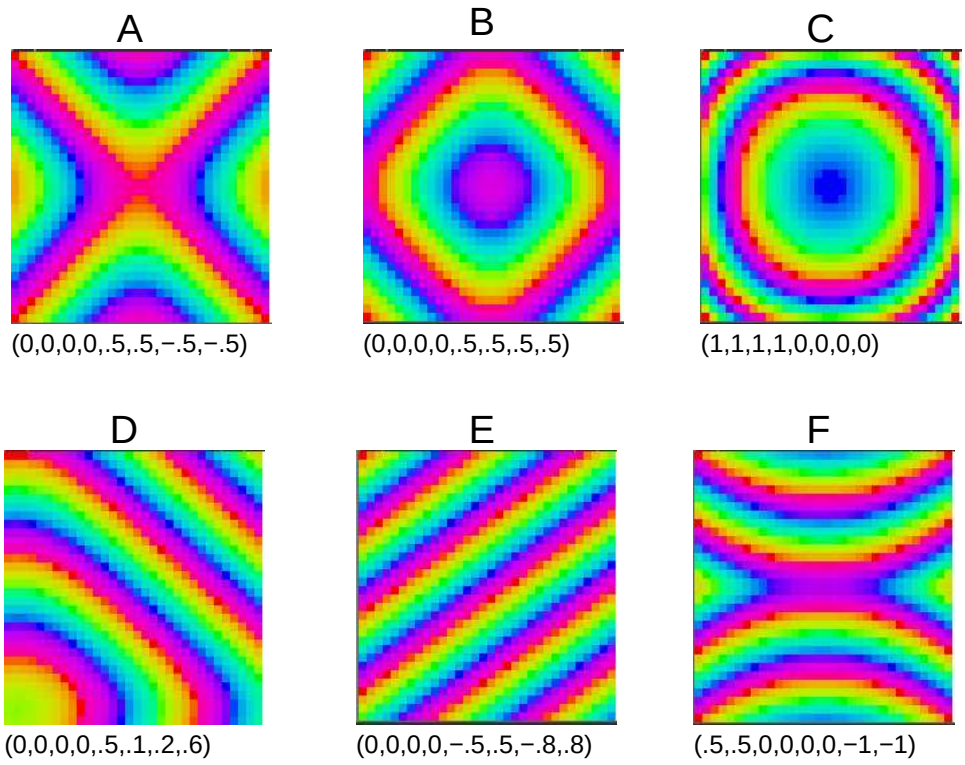

Figure 6: Steady state phase relative to the upper-left oscillator in 32×32 arrays of locally coupled oscillators. Coupling is through a function of the form $A_0 + A_1 \cos\theta + B_1 \sin\theta$. Each of the four cardinal directions can be different. $B_1 = 1$ in all cases. Parameters in the parentheses correspond to $(A_0^E, A_0^W, A_0^S, A_0^N, A_1^E, A_1^W, A_1^S, A_1^N)$.

are not branches of the synchronous state? For example, *in a ring*, the traveling wave solutions are topologically different from the synchronous solution and thus cannot be continued from that trivial branch. One analogue of such a pattern in two-dimensions is a spiral wave. Some of these waves are illustrated in figure 7. Figure 7A is a solution to the highly symmetric system:

$$\theta'_{jk} = \omega + \sum_{j',k'} \sin(\theta_{j',k'} - \theta_{jk})$$

where the sum is over the four nearest neighbors, {N,S,E,W}. In [49], we showed that there is a rotating wave-solution to this equation and with theorem 1, that it is asymptotically stable. Here is an example of the distribution of the phases for the 4×4 case:

$$\begin{array}{cccc} 0 & \xi & \pi/2 - \xi & \pi/2 \\ -\xi & 0 & \pi/2 & \pi/2 + \xi \\ 3\pi/2 + \xi & 3\pi/2 & \pi & \pi - \xi \\ 3\pi/2 & 3\pi/2 - \xi & \pi + \xi & pi \end{array}$$

The reader is urged to check that there is a $\xi \in (0, \pi/4)$ which leads to a phaselocked solution and that this solution is stable. If we replace $H(u) = \sin u$ with the more general, $H(u) = \sin u + d(\cos u - 1)$, then the rotatinmg wave develops a twist and looks more like a spiral wave. Figure 7B shows such a spiral wave. As d increases, the spiral becomes tighter and tighter until eventually, the phase differences near the center become too great. The spiral disappears and leaves a "gently wobbling" spiral in its wake. Larger values of d result to large scale meandering of the spiral; a snapshot is shown in Figure 7C. Figure 7D shows another solution with the same parameters as in figure 7B, but with random initial data. There are many apparently stable steady state phaselocked solutions which consist of random arrangements of phase singularities.

6 Neural networks.

The previous sections dealt with networks of single neurons which were coupled together using chemical synapses. In this section, we are interested in firing-rate models; that is models of neurons in which the actual times of spikes are not specified. Rather, we specify the average firing rates of a neuron or a population of neurons. There are many different derivations of these firing rate models and we suggest that the reader consult [18, 15] for a general survey of formal means of obtaining the equations. We will present one method of deriving them that is tightly connected to the underlying biophysics of the neuron. Our method entails the use of a slow time scale in order to reduce a single neuron to a one (and possibly two) variable equation.

6.1 Slow synapses

For simplicity, we consider a simple network with one excitatory cell which has slow spike-frequency adaptation (which we can always set to zero) with self-

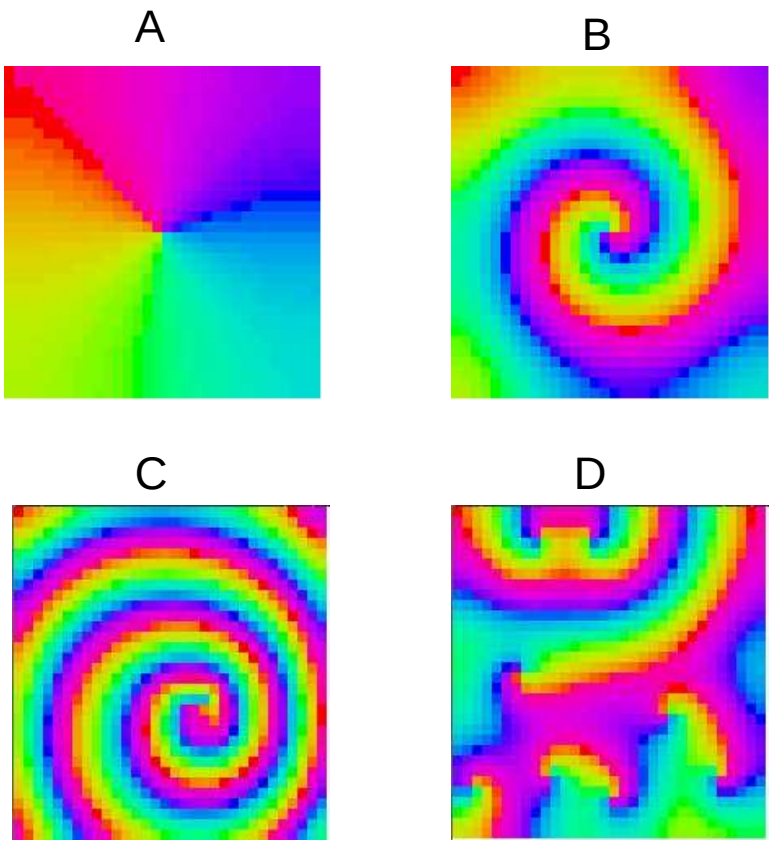

Figure 7: Spiral waves in a locally coupled 32×32 oscillator array. (A) Pure sinusoidal coupling. (B) Coupling with $H(\theta) = \sin\theta + .6(1 - \cos\theta)$. (C) With a cosine component of 0.8, locking is no longer possible and the core of the spiral wobbles as shown in this snapshot. (D) Same parameters as (B) but with random initial data.

coupling and one inhibitory neuron which also is coupled to itself as well as to the excitatory cell. (The reason for self-coupling is to give the most general formulation of the reduction.) The derivation then suggests how to couple whole networks of neurons.

We start with the following system:

$$\begin{aligned} C\frac{dV_e}{dt} &= -I_{fast,e}(V_e,\ldots) - g_{ee}s_e(V_e-E_e) - g_{ie}s_i(V_e-E_i) \quad (17)\\ &- g_z z(V_e-E_z) + I_e \\ C\frac{dV_i}{dt} &= -I_{fast,i}(V_i,\ldots) - g_{ei}s_e(V_i-E_e) - g_{ii}s_i(V_i-E_i) + I_i \quad (18)\\ \frac{ds_e}{dt} &= \alpha_e(V_e)(1-s_e) - s_e/\tau_e \quad (19)\\ \frac{ds_i}{dt} &= \alpha_i(V_i)(1-s_i) - s_i/\tau_i \quad (20)\\ \frac{dz_e}{dt} &= \alpha_z(V_e)(1-z_e) - z_e/\tau_z \quad (21) \end{aligned}$$

The first two equations represent the potentials of the excitatory and inhibitory cells respectively. The terms $I_{fast,*}$ may involve many additional variables such as the transient sodium and delayed rectifier channels necessary for spiking. The $s_{e,i}$ variables gate the synapses between the neurons and lie between 0 (fully closed) and 1 (fully open). The functions $\alpha_{e,i}$ are zero unless the neuron is spiking and then they are some finite value. $\tau_{e,i}$ are the time constants for the decay of the synapses. The parameters g_{jk} represent the maximal conductances of the synapses and $E_{e,i}$ are the reversal potentials of the excitatory and inhibitory synapses. Typically E_e =0 mV and $E_i = -70$ mV although this latter value can be closer to -85 mV or up to -60 mV. The variable z gates the degree of spike-frequency adaptation for the excitatory cell; the function $\alpha_z(V)$ and the parameters, τ_z, g_z, and E_z are similar to those of the synapses.

In order to perform the needed reduction, we assume that $s_{e,i}$ and z are all much slower than the fast system. Thus, we can treat them as parameters. We assume that the fast dynamics of both excitatory and inhibitory cells is such that as current is increased, the neuron switches from a stable fixed point to large magnitude periodic firing. Furthermore, we also assume that the neuron is monostable so that there are no currents for which it can both stably oscillate and remain at rest. For example, if the fast-dynamics is class I, then as the current increases the fixed point diappears at a saddle-point and large-amplitude periodic oscillations emerge. Consider the excitatory dynamics :

$$\frac{dV_e}{dt} = -I_{fast,e}(V_e,\ldots) - G_{ee}(V_e-E_e) - G_{ie}(V_e-E_i) - G_z(V_e-E_z) + I_e$$

where G_{ee}, G_{ie}, G_z are parameters. Let

$$I(V; G_{ee}, G_{ie}, G_z, I_e) = -G_{ee}(V_e-E_e) - G_{ie}(V_e-E_i) - G_z(V_e-E_z) + I_e$$

be the applied current. Holding (G_{ee}, G_{ie}, G_z) constant, we suppose that as the applied current is increased, there is a saddle-node at $I_e^*(G_{ee}, G_{ie}, G_z)$. For

$I_e < I_e^*$ the neuron is at rest and for $I_e > I_e^*$ the neuron fires repetitively with a frequency

$$f_e \approx \beta_e \sqrt{I_e - I_e^*}.$$

Now, we are ready for the reduction. Consider equation (19). If $I_e < I_e^*$ then the neuron is not firing and $\alpha_e(V_e) = 0$. If $I_e > I_e^*$, then the neuron fires repetitively with period, $T_e = 1/f_e$. We have assumed that this is fast compared to the dynamics of the synapse so that we can average the s_e dynamics obtaining

$$\frac{ds_e}{dt} = f_e \left[\int_0^{T_e} \alpha_e(V_e(t))\ dt \right] (1 - s_e) - s_e/\tau_e.$$

(We have used the fact that $1/T_e = f_e$.) For many neural models, the spike-width is nearly independent of the frequency, so that the integral can be approximated as a constant independent of T_e, say, a_e. Using the frequency approximation, we see that

$$\frac{ds_e}{dt} = a_e \beta_e \sqrt{I_e - I_e^*}(1 - s_e) - s_e/\tau_e$$

when $I_e > I_e^*$. We recall that I_e^* is a function of (G_{ee}, G_{ie}, G_z) which are given by $(g_{ee}s_e, g_{ie}s_i, g_z z)$. Thus, to close the system, we need an expression for I_e^*. Numerically, for a wide variety of models, one finds that typically

$$I_e(G_{ee}, G_{ie}, G_z) \approx G_{ee}U_{ee} - G_{ie}U_{ie} - G_z U_z - I_{\theta,e}$$

where U_{ee}, U_{ie}, U_z are positive constants which have the dimension of potential and $I_{\theta,e}$ is the threshold current to initiate repetitive spiking in absence of any slow conductances. Assuming the fast dynamics of the excitatory and inhibitory cells are similar, we have reduced equations (17- 21) to the following three equations

$$\frac{ds_e}{dt} = c_e F(I_e + I_{ee}s_e - I_{ie}s_i - I_z z - I_{\theta,e})(1 - s_e) - s_e/\tau_e \tag{22}$$

$$\frac{ds_i}{dt} = c_i F(I_i + I_{ei}s_e - I_{ii}s_i - I_{\theta,i})(1 - s_i) - s_i/\tau_i \tag{23}$$

$$\frac{dz}{dt} = c_z F(I_e + I_{ee}s_e - I_{ie}s_i - I_z z - I_{\theta,e})(1 - z) - z/\tau_z, \tag{24}$$

where $F(x) = \sqrt{\max(x, 0)}$, $c_e = a_e\beta_e, c_z = a_z\beta_e, c_i = a_i\beta_i$ and $I_{ee} = g_{ee}U_{ee}$ and so on for the other I_{jk}.

Before continuing with our analysis of these models, we introduce a smoothed version of the function F. Numerous authors have shown that the presence of noise changes a sharp threshold for firing to a smoother and more graded firing rate. In a recent paper, [44] analyzed the firing properties of the normal form for a saddle-node. Using standard stochastic methods, they derive a complicated integral form for the firing rate curve as a function of the amount of noise. We find that a good approximation of such a curve is given by the smooth function:

$$F(I) = \sqrt{\log(1 + \exp(I/b))b}$$

where b characterizes the amount of "noise." That is, as $b \to 0^+$, F approaches the deterministic model. In the analysis below, we use $b = 0.1$.

6.2 Analysis of the reduced model.

We sketch some possible types of solutions to the reduced network model. This is by no means exhaustive

6.2.1 Purely excitatory with no adaptation.

When there is no feedback inhibition and the adaptation is blocked, the equations reduce to

$$\frac{ds_e}{dt} = c_e F(I_e + I_{ee} s_e - I_{\theta,e})(1 - s_e) - s_e/\tau_e.$$

This is a one-dimensional system so that there are only fixed points. Since $F \geq 0$, the interval $[0, 1]$ is positively invariant so there exists at least one stable fixed point. Suppose, $I_{ee} = 0$ so there is no recurrent excitation. Then the fixed point is unique:

$$\bar{s}_e = \frac{c_e F(I_e - I_{\theta,e})}{c_e F(I_e - I_{\theta,e}) + 1/\tau_e}.$$

For small enough I_{ee} the fixed point persists and remains stable. Further increases in I_{ee} can lead to a fold bifurcation and the annihilation of the fixed point. But since we know there is always at least one fixed point, then there must in general (except at bifurcation points) be an odd number. Since this is a scalar system and the function F is continuous, the fixed points alternate in stability. For many choices of F, there is bistable behavior representing the neuron firing at a low or zero rate and at a much higher rate.

6.2.2 Excitatory with adaptation.

The presence of spike adaptation enables the network to oscillate and also allows it to be excitable. We point out that oscillations in s_e at the slow time scale assumed here correspond to bursting oscillations of the original model system. Baer et al [2] analyzed a slow two-variable system which modulates a fast spiking system through a saddle-node bifurcation and used this as a model for parabolic bursting. A rigorous analysis of a saddle-node that is slowly periodically driven was provided by Ermentrout and Kopell [22]. Figure 8 shows the bifurcation diagram for a set of parameters as the drive increases. Figure 8B shows the network in an excitable regime; weak stimuli lead to a decay to rest while stronger stimuli cause a burst of activity. Increasing the drive leads to a subcritical Hopf bifurcation and bistability between a large amplitude periodic orbit and a fixed point (Figure 8C). Further increases in the drive lead to a single stable periodic orbit (figure 8D).

6.2.3 Excitatory and inhibitory.

If we remove the adaptation, but allow inhibition, then we are in the case considered in the classic Wilson-Cowan model. This scenario has been explored thoroughly by many authors [3, 18]. The phaseplane possibilities are very close

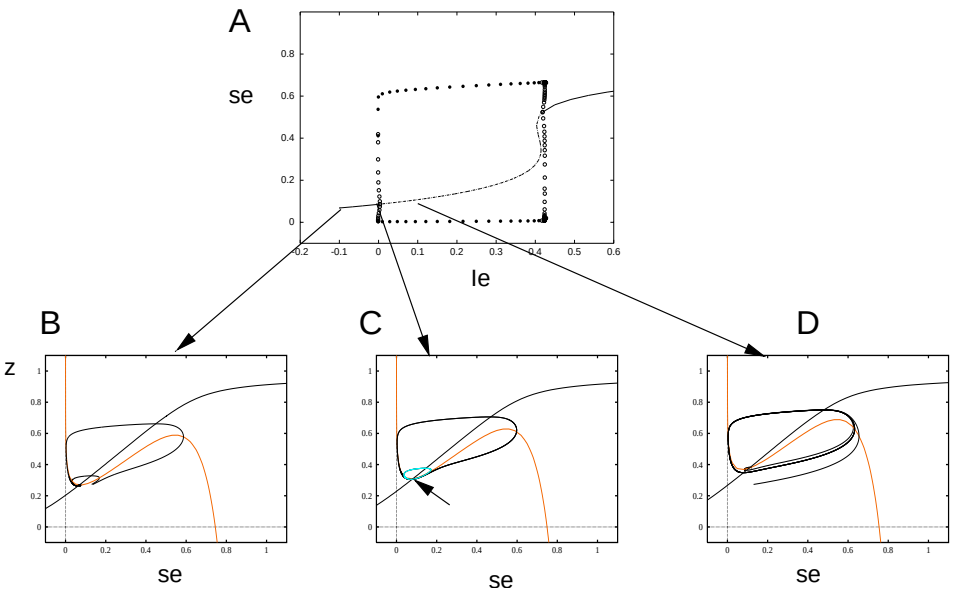

Figure 8: Example behavior of a self-coupled excitary cell with adaptation. (A) The bifurcation diagram as the driving current, I_e increases. (B,C,D) three sample phaseplanes at different driving currents showing excitability (B), bistability (C), and periodic orbits (D). In (C), arrow shows the stable fixed point and the small blue curve shows the unstable periodic orbit.

to those of the excitatory-adaptation model. There is more flexibility in the placement of the nullclines since the inhibitory cells receive inputs independent of the excitatory population. That is, there is the possibility for *feedforward* rather than feedback inhibition.

6.2.4 Full model.

Since the model is three variables, complex behavior is a possibility. For example if the adaptation is slow, then it can slowly move the excitatory-inhibitory "fast" system back and forth through bifurcations producing bursting [35].

6.3 Spatial models.

We can take the reduced model described in the previous section and create a spatially distributed network in order to understand the kinds of behavior in a one-dimensional slice of cortex. Consider the following spatial analogue of equations (22-24):

$$\begin{aligned}
\frac{\partial s_e}{\partial t} &= c_e F(I_e + I_{ee} J_{ee} * s_e - I_{ie} J_{ie} * s_i - I_z z - I_{\theta,e})(1 - s_e) - s_e/\tau_e \quad (25)\\
\frac{\partial s_i}{\partial t} &= c_i F(I_i + I_{ei} J_{ei} * s_e - I_{ii} J_{ii} * s_i - I_{\theta,i})(1 - s_i) - s_i/\tau_i \\
\frac{\partial z}{\partial t} &= c_z F(I_e + I_{ee} J_{ee} * s_e - I_{ie} J_{ie} * s_i - I_z z - I_{\theta,e})(1 - z) - z/\tau_z,
\end{aligned}$$

where

$$J * u \equiv \int_\Lambda J(x - y) u(y, t)\, dy.$$

In general, these spatial interaction functions are normalized so that the integral over the domain, Λ, is one. For the purposes of analysis, we will assume that the domain is the real line, a circle, the plane, or a torus. In the cases of a torus or a circle, the functions $J(x)$ will be periodic.

6.3.1 Bistability and fronts.

As in the previous section, we first consider the purely excitatory case so that the equations are simply:

$$\frac{\partial s_e}{\partial t} = c_e F(I_e + I_{ee} J_{ee} * s_e)(1 - s_e) - s_e/\tau_e. \quad (26)$$

Suppose that $g(u) \equiv c_e F(I_e + I_e e u)(1 - u) - u/\tau_e$ has three roots. That is, suppose that the spatially homogeneous excitatory network is bistable. Then, as in the case of the bistable scalar reaction-diffusion equation, we expect that there may be front solutions joining one stable rest state to another. In fact, for the present model if we assume that J_{ee} is symmetric, positive, and has an integral of 1, then a theorem of Chen [8] implies that there exists a unique traveling front solution, $s_e(x, t) = S(x - ct)$ with velocity, c joining the two stable fixed points. We illustrate such a solution in figure 9A.

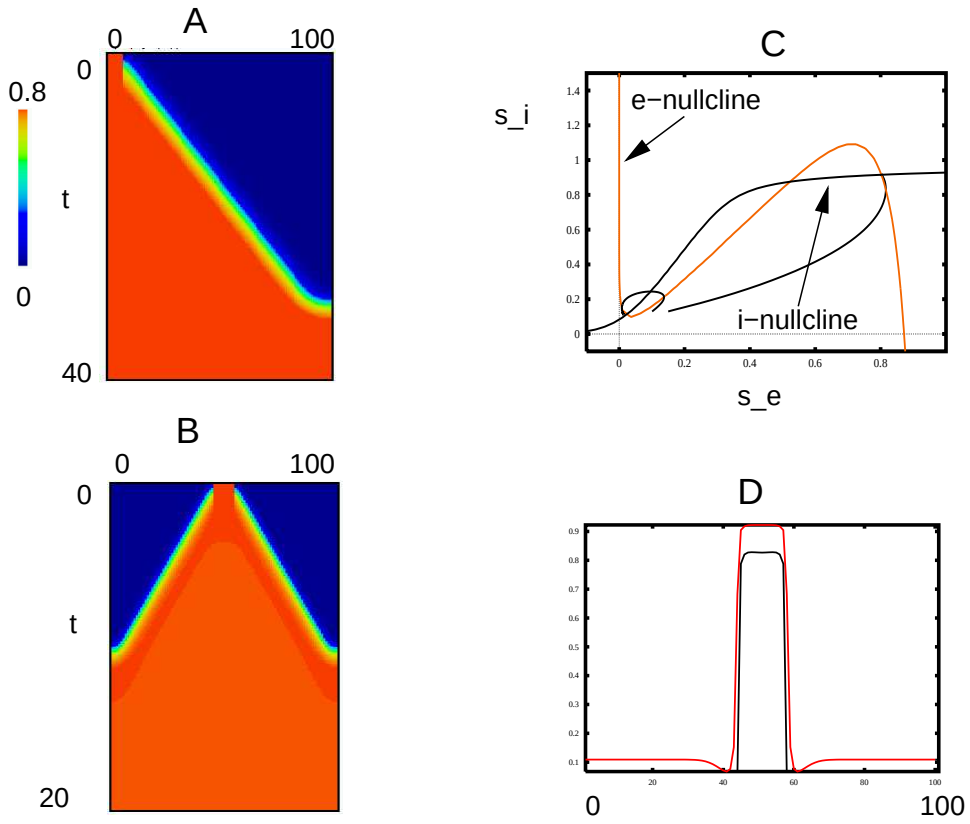

Figure 9: Bistable media. (A) Space-time plot of a front for the scalar equation (26). Color scale is amplitude of $s_e(x,t)$ with time running vertically and space horizontally. $J_{ee} = \exp(-|x|/\sigma)/(2\sigma)$ with $\sigma = 2$. (B) Space-time plot for a network with excitation and inhibition with local dynamics as in (C). The spatial interactions are exponential with $\sigma_i = 1, \sigma_e = 2$. (C) Phaseplane for the $s_e - s_i$ system with no adaptation showing bistability. (D) Stationary localized bumps in the same parameter set as (B) but with excitation slowed by a factor of 2 and $\sigma_e = 1, \sigma_i = 2.5$. Horizontal axis indicates spatial index and the black and red curves are s_e, s_i respectively.

6.3.2 Fronts and localized excitation in the presence of inhibition.

Figure 9B illustrates a front produced in a two-population network whose null-cline configuration is illustrated in figure 9C. Here we have turned off the adaptation so that $I_z = 0$. Unlike figure 9A, we have initiated the excitation in the center of the medium. Clearly, there is still a front which propagates but the rigorous existence of this front remains to be proven. Unlike the scalar system, however, the properties of bistability alone are not sufficient to guarantee a wave front. In particular, the time constant and the spatial extents matter in two-population models. Figure 9D illustrates a stationary localized solution to the excitatory-inhibitory network where we have slowed the excitation down by a factor of two and given the inhibitory cells a spatial extent two-and-a-half times that of the excitatory cells. Localized pulses have been the subject of numerous theoretical and numerical studies since the first rigororous analysis of this problem by Amari [1]. These pulses are thought to represent working or short-term memory [62]. Pinto and Ermentrout [50] used sigular perturbation (treating the extent of inhibition, σ_i, as a large parameter) to contruct solitary pulses in an excitatory-inhibitory network of the prsent form. Their starting point assumes the existence of fronts

6.3.3 Propagating pulses.

Suppose that we eliminate the inhibition. In experimental slice preparations, this is a common protocol in order to study the excitatory connectivity. We maintain the spike adaptation, z, and suppose that we have the phaseplane depicted in Figure 8A (and repeated in 10A). Then, instead of fronts as in figure 9A, we obtain traveling pulses as shown in Figure 10B. Essentially, if the adaptation is slow, then this can be regarded as a singular perturbation problem. For a fixed level of adaptation, the excitatory network is bistable and produces fronts between high and low levels of activity as in figure 9. Thus, this pulse can be viewed as a front and a "back" joined at a level of adaptation leading to the same speed. In other words, these localized traveling pulses are analogous to singular perturbation constructions of pulses in reaction-diffusion equations [7]. Indeed, Pinto and Ermentrout [51] use such a singular perturbation argument to construct these fronts.

In the scenario described above, the local dynamics is excitable; there is a single globally stable fixed point. However, the excitability of the medium depends on the slow dynamics of the adaptation. This type of excitability is called Class II in the context of single neuron models ([54];see also figure 1B in the present article). Suppose that there is no adaptation, but instead, we allow inhibition. Then Class II excitability is still possible, but another type of excitability is now possible. Figure 10C shows the phaseplane for the excitatory-inhibitory network with no adaptation. Unlike the phaseplane in figure 10A, there are three fixed points. However, the rightmost fixed point is unstable. The middle fixed is a saddle-point whose unstable manifolds form a heteroclinic loop with the leftmost stable fixed point. Thus, we have the

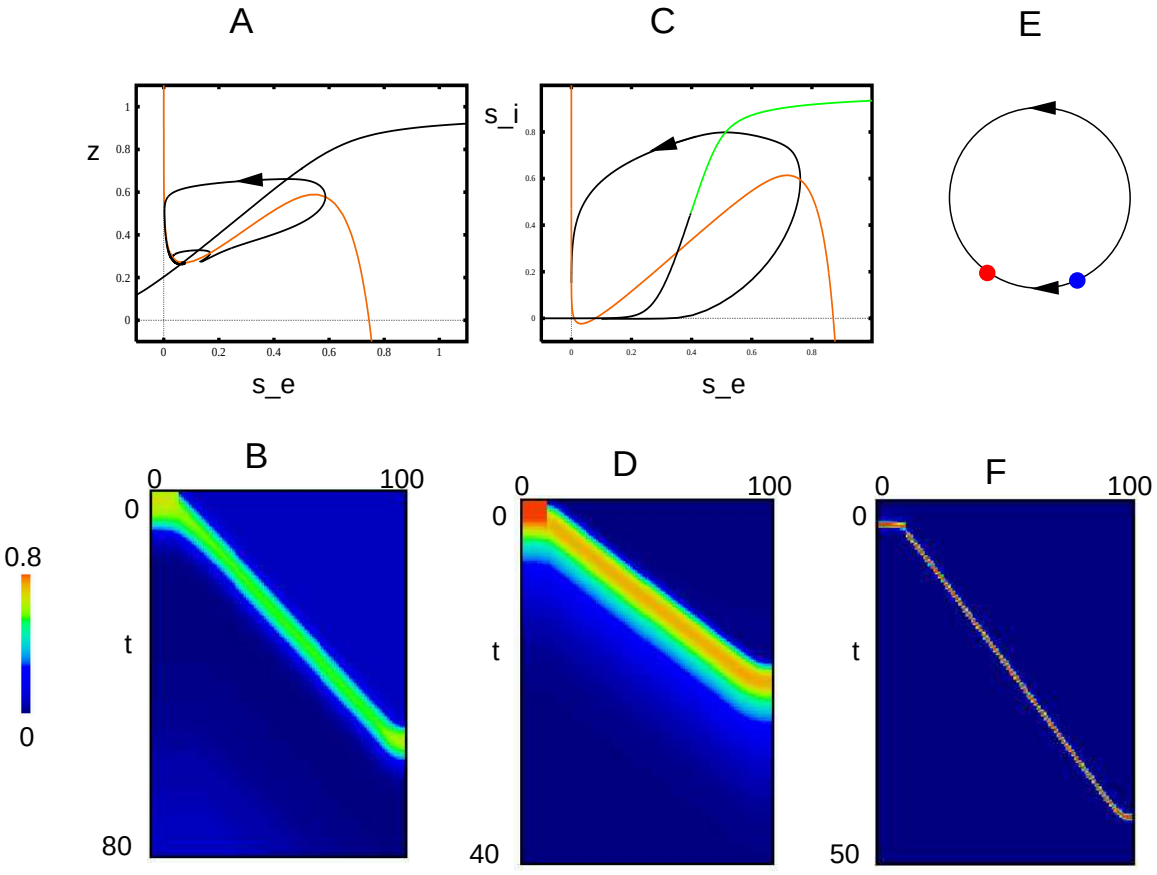

Figure 10: Propagation of solitary pulses in an excitable network. (A) Phase-plane for a system with no inhibition showing excitable behavior. (B) Behavior of a network of 101 cells with exponentially decaying connectivity with local dynamics as in (A). $s_e(xt)$ is plotted with time increasing downward. (C) Excitable system with no adaptation and just inhibitory and excitatory cells. Note that there are three fixed points; only the leftmost one is stable. (D) Behavior of a network of excitatory and inhibitory cells where $\sigma_e = 4$ and $\sigma_i = 2$. (E) Ring model with two fixed point as a simple version for the dynamics in (C). (F) Solution to equation (27); $P(\theta)$ is plotted since this represents the actual activity.

analogue of class I excitability as shown in figure 1C. The stable manifolds of the saddle point provides a true threshold; it is not necessary to have widely different timescales between the two variables to achieve excitability. Figure 10D shows the behavior of a network with excitatory and inhibitory neurons whose local dynamics is that of 10C. There has been little analysis of this type of network excitability. However, we offer a simple approximation leading to a scalar problem which may be amenable to analysis. The dynamics of the pulse is largely confined to a tubular neighborhood of the unstable manifolds of the saddle-point which form a ring. This suggests a scalar "ring model" for the local dynamics as shown in figure 10E. Ermentrout and Rinzel [27] used such a ring model to study propagation in a reaction-diffusion excitable system. Consider the following system:

$$\frac{\partial \theta(x,t)}{\partial t} = F[\theta(x,t)] + gR[\theta(x,t)] \int_\Lambda J(x-y)P[\theta(y,t)]\ dy. \tag{27}$$

The functions F, R, P are , say, $2\pi-$periodic functions of their arguments. The function: $q(u) = F(u) + R(u)P(u)$ characterizes the ring dynamics. We assume that there are two fixed points, u_s and u_t representing the stable fixed point and the threshold respectively. Since q is periodic, there is also a fixed point, $u_s + 2\pi$. The function R represents the response of the ring model to inputs; since this is a class I system, R will usually be non-negative. The function $P(u)$ is the shape of the pulse of activity; it is positive and narrowly peaked. We assume that $R(u_s) > 0$ so that inputs to a resting cell will excite it past threshold. We can ask whether the scalar problem, equation (27), admits a traveling *front* solution joining u_s to $u_s + 2\pi$. Note that since the phase space is a ring, this actually represents a traveling pulse. Osan et al [48] studied a similar system but in the context of single neurons and with a time-dependent synapse replacing the function $P(u)$. Figure 10E shows a simulation of a network of 101 cells with $J(x)$ exponential, $R(u) = 1 + \cos u$, $P(u) = (.5 + .5\cos(u - 2.5))^5$, $F(u) = .98 - 1.02\cos(u)$ and $g = 2.2$. Since θ is a front, we plot $P(\theta)$ instead since these are the real coordinates. Despite the similarity of (27) to (26), we cannot apply Chen's theorem to the former. The reason for this is that one of the assumptions of the Chen theorem is equivalent to $P'(u) \geq 0$. Since P is a pulse-like function, this assumption will be violated. The precise conditions for the existence of solutions like figure 10E for (27) remain to be determined.

6.3.4 Oscillatory networks.

Consider the excitatory-inhibitory network with no adaptation. Suppose that we are in the same local configuration as figure 10C and drive the excitatory cells enough so that the lower two fixed points merge and disappear. Then, the local network oscillates. Figure 11A shows the phaseplane of the EI system with no adaptation. Now suppose that we couple the network with exponentially decaying functions for which the excitation spreads more than the inhibition ($\sigma_e > \sigma_i$). Then, as seen in figure 11B, the network generates waves which eventually synchronize. However, if the inhibition spreads farther than the

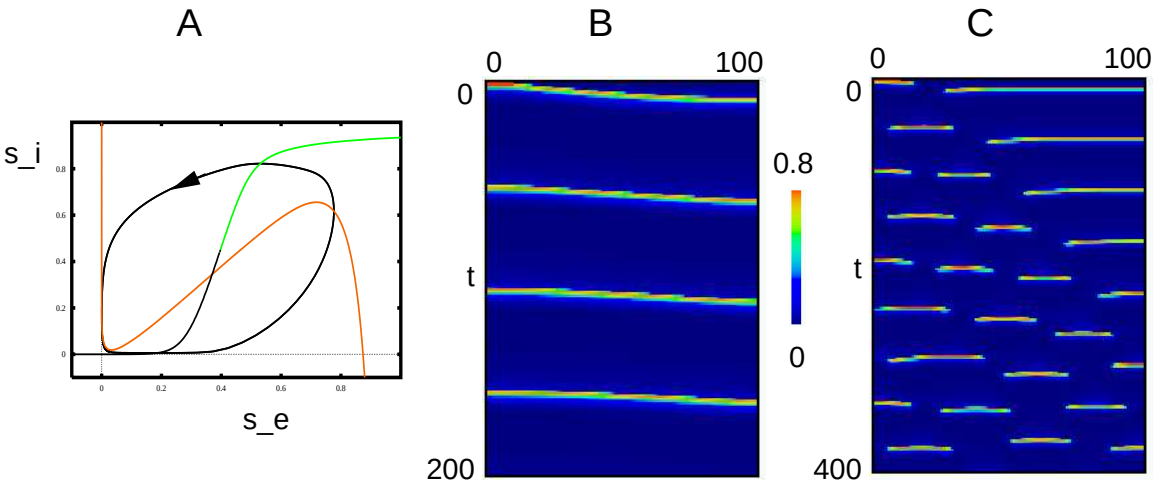

Figure 11: Oscillatory E-I network. (A) Phaseplane for the local dynamics showing the existence of a stable limit cycle. (B) A network where $\sigma_e = 2$ and $\sigma_i = 1$. s_e, s_i are initialized at identical low value. The first 10 excitatory cells are raised to a value of 1 inducing a wave of activity. The network oscillates and tends to a synchronous solution. (C) Same as (B), but σ_i is raised to 4 leading to an instability of the synchronous state and the appearance of clustered solutions

excitation, the synchronous solution is no longer the unique stable solution. One such non-synchronous solution is illustrated in figure 11C; the network breaks up into clustered states. Other initial data lead to synchrony so that this network seems to be bistable.

6.3.5 Turing-type instabilities.

As a final example of spatial effects on networks, we consider a system where *all* of the interesting dynamics arises due to the spatial interactions. That is, the local dynamics consists of a single stable fixed point with no excitability. We now connect this up with long-range inhibition and short-range excitation. This is the classical scenario for pattern formation and results in an instability of the uniform state to a nonzero wave number. We sketch the basic ideas of the analysis. Let $\bar{s_e}, \bar{s_i}$ be a spatially uniform fixed point to equation (25) when there is no adaptation. Write $s_e = \bar{s_e} + u$ and $s_i = \bar{s_i} + v$. The linearized system has the form

$$\frac{\partial}{\partial t}\begin{pmatrix} u \\ v \end{pmatrix} = \begin{pmatrix} -c_{ee}u + d_{ee}J_{ee} * u & -d_{ie}J_{ie} * v \\ d_{ei}J_{ei} * u & -c_{ii}v - d_{ii}J_{ii} * v \end{pmatrix}$$

Since the rest state is on the middle branch, this means that $-c_{ee} + d_{ee} > 0$ so that $d_{ee} > 0$. All of the other coefficients are obviously non-negative. Suppose that we work on the infinite domain. Then solutions to this linear problem have

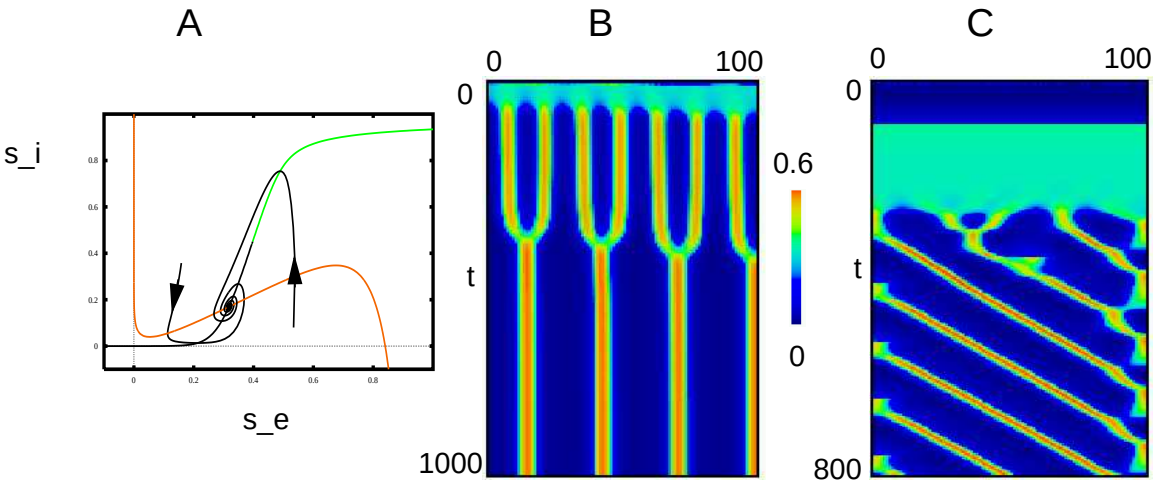

Figure 12: The Turing instability. (A) The phaseplane for the local dynamics; there is a stable fixed point on the middle branch. (B) The same system generates spatial stationary patterns due to the long-range inhibition; $\sigma_e = 2.0, \sigma_i = 7.5$. (C) Some of the inhibition is removed and an equal amount of adaptation is added to compensate. The rest state of the local dynamics is still stable. However, the same spatial interactions as in (B) lead to a destabilization of the rest state through a Hopf bifurcation and a nonzero wave number. The spatial patterns become traveling waves.

the form:

$$[u(x,t), v(x,t)] = e^{ikx+\lambda(k)t}[\bar{u}, \bar{v}]$$

where $k \geq 0$. $\{\lambda(k); [\bar{u}, \bar{v}]\}$ is a eigenvalue-eigenvector pair for the matrix:

$$M(k) \equiv \begin{pmatrix} -c_{ee} + d_{ee}\hat{J}_{ee}(k) & -d_{ie}\hat{J}_{ie}(k) \\ d_{ei}\hat{J}_{ee}(k) & -c_{ii} - d_{ii}\hat{J}_{ii}(k) \end{pmatrix}$$

where

$$\hat{J}(k) = \int_{-\infty}^{\infty} J(x)e^{-ikx}\ dx.$$

We note that if J is an exponential or Gaussian, then $\hat{J}$ is non-negative and decreases with $|k|$. If $M(k)$ has eigenvalues with positive real parts for some k, then the rest state is unstable and perturbations with this wavelength will tend to grow. This sets the template for patterns for the full nonlinear system [46]. Since M is a 2×2 matrix, stability is guaranteed if the trace is negative and the detrminant positive. If we suppose that $J_{ee} = J_{ei} = J_e$ and $J_{ie} = J_{ii} = J_i$, then, the trace, δ and the determinant, Δ satisfy:

$$\begin{aligned} \delta(k) &= -(c_{ii} + c_{ee}) + d_{ee}\hat{J}_e(k) - d_{ii}\hat{J}_i(k) \\ \Delta(k) &= c_{ee}c_{ii} + (d_{ie}d_{ei} - d_{ii}d_{ee})\hat{J}_e(k)\hat{J}_i(k) - c_{ii}d_{ee}\hat{J}_e(k) + c_{ee}d_{ii}\hat{J}_i(k). \end{aligned}$$

At $k = 0$, we know that the rest state is stable and for k large, all $k-$dependent terms vanish so that the rest state is stable to large k perturbations. However, because $d_{ee} > 0$ it is possible for intermediate values of k to produce instabilities. This point is critical: if the rest state is not on the increasing middle-branch of the E-nullcline, then no spatial instabilities are possible. If the self-inhibition is weak, then d_{ii} is small and the trace will be negative for $k > 0$ if it is negative for $k = 0$ as assumed. Consider for simplicity the case where $d_{ii} = 0$. Then the trace is a monotonically decreasing function of k and since it is assumed to be negative when $k = 0$, the trace is always negative. On the other hand, the determinant can become negative if d_{ee} is large enough since the term $\hat{J}_e(k)\hat{J}_i(k)$ decreases more rapidly than $\hat{J}_e(k)$. Such a scenario can then lead to an instability as an eigenvalue crosses through zero at some non-zero k. Figure 12B illustrates as example of this instability for the full nonlinear system. Two-dimensional analogues of this instability were suggested as a mechanism for visual hallucinations in Ermentrout and Cowan [19].

Suppose that we include adaptation as well as inhibition. We can remove some of the inhibition to compensate for the presence of adaptation which acts like a local slow inhibition. Figure 12C shows the result of this; instead of stationary patterns of activity, we obtain traveling waves. What is surprising about these waves is that the domain is finite and the boundaries seem to have little influence on the waveform.

References

[1] Amari, S, 1977, Dynamics of patternformation in lateral-inhibition type neural fields, Biol. Cybernet. 27:77-87.

[2] Baer, S.M., J. Rinzel, and H. Carrillo: Analysis of an autonomous phase model for neuronal parabolic bursting. J. Math. Biol. 33:309-333 (1995).

[3] Beer, R. On the Dynamics of Small Continuous-Time Recurrent Neural Networks, Adaptive Behavior, 3:469-509, 1994.

[4] P.D. Brodfuehrer, E.A. Debski, B.A. O'Gara, and W.O. Friesen, 1995, Neuronal control of leech swimming, J. Neurobiology, 27:403-418.

[5] Buck, J., 1988, Synchronous rhythmic flashing in fireflies, II. Q. Rev. Biol. 63:265-289.

[6] P.L. Buono and M. Golubitsky. Models of central pattern generators for quadruped locomotion: I. primary gaits. J. Math. Biol. 42 (4) (2001) 291-326.

[7] Casten RG, Cohen H, Lagerstrom PA (1975) Perturbation analysis of an approximation to the Hodgkin-Huxley theory. *Quart. J. Appl. Math.* 32(4):365–402.

[8] Chen, X, Existence, Uniqueness, and Asymtotic Stability of Traveling Waves in Nonlocal Evolution Equations, Advances in Differential Equations 2, 125-160 (1997)

[9] Chen, Z and Ermentrout, B Wave Propogation Mediated by $GABA_B$ Synapse and Rebound Excitation in an Inhibitory Network: A Reduced Model Approach, Journal of Computational Neuroscience 5, 53-69 (1998).

[10] C.C. Chow and N. Kopell, 'Dynamics of spiking neurons with electrical coupling', Neural Comp. **12**, 1643-1678 (2000).

[11] Chow, CC. Phaselocking in weakly heterogeneous neuronal networks. Physica D 118:343-370 (1998).

[12] A.H. Cohen, S. Rossignol, and S. Grillner, 1988, Neural Control of Rhythmic Movements in Vertebrates, New York, Wiley.

[13] Cohen AH, Ermentrout GB, Kiemel T, Kopell N, Sigvardt KA, Williams TL. Modelling of intersegmental coordination in the lamprey central pattern generator for locomotion. Trends Neurosci. 1992 Nov; 15(11):434-8.

[14] Crook, S and A Cohen. (1995) Central pattern generators. In Bower and Beeman, editors, The Book of GENESIS: A workbook of tutorials for the GEneral NEural SImulation System, Chapter 6.

[15] Dayan, P. and Abbott, L. Theoretical Neuroscience, 2001, MIT Press, Cambridge MA, Chapt 7.

[16] Ermentrout,-G.-Bard, Stable periodic solutions to discrete and continuum arrays of weakly coupled nonlinear oscillators. SIAM-J.-Appl.-Math. 52 (1992), no. 6, 1665-1687.

[17] Ermentrout-B, Linearization of F-I curves by adaptation. Neural-Comput. 1998 Oct 1; 10(7): 1721-9

[18] Ermentrout-B, Neural networks as spatio-temporal pattern-forming systems, Reports on Progress in Physics, 61:353-430, 1998.

[19] Ermentrout,-G.-B.; Cowan,-J.-D., A mathematical theory of visual hallucination patterns. Biol.-Cybernet. 34 (1979), no. 3, 137-150.

[20] Ermentrout-B; Flores-J; Gelperin-A, Minimal model of oscillations and waves in the Limax olfactory lobe with tests of the model's predictive power. J-Neurophysiol. 1998 May; 79(5): 2677-89

[21] Ermentrout, G.B. Kopell, N. Frequency plateaus in a chain of weakly coupled oscillators. I. 1984 SIAM-J.-Math.-Anal. 15 (1984), no. 2, 215–237.

[22] Ermentrout,-G.-B.; Kopell,-N., Parabolic bursting in an excitable system coupled with a slow oscillation. SIAM-J.-Appl.-Math. 46 (1986), no. 2, 233-253.

[23] Ermentrout G.B. and Kopell, N 1991, Multiple pulse interactions and averaging in systems of coupled neural oscillators, J. Math. Biology 29:195-217

[24] Ermentrout GB, Kopell N. Fine structure of neural spiking and synchronization in the presence of conduction delays. Proc Natl Acad Sci U S A. 1998 Feb 3;95(3):1259-64.

[25] Ermentrout GB, Kleinfeld D Traveling electrical waves in cortex: insights from phase dynamics and speculation on a computational role NEURON 29: (1) 33-44 JAN 2001

[26] Ermentrout B, Pascal M, Gutkin B The effects of spike frequency adaptation and negative feedback on the synchronization of neural oscillators NEURAL COMPUT 13 (6): 1285-1310 JUN 2001

[27] Ermentrout,-G.-Bard; Rinzel,-John, Waves in a simple, excitable or oscillatory, reaction-diffusion model. J.-Math.-Biol. 11 (1981) 269-294.

[28] Ermentrout B, Wang JW, Flores J, and Gelperin, A. Model for olfactory discrimination and learning in Limax procerebrum incorporating oscillatory dynamics and wave propagation J NEUROPHYSIOL 85 (4): 1444-1452 APR 2001

[29] W. Gerstner, J.L. van Hemmen, and J. Cowan. What matters in neuronal locking? Neural Comp. **8** 1653-1676 (1996).

[30] Goel P, Ermentrout B Synchrony, stability, and firing patterns in pulse-coupled oscillators PHYSICA D 163 (3-4): 191-216 MAR 15 2002

[31] C.M. Gray, 1994, Synchronous oscillations in neuronal systems: mechanisms and functions, J. Computat. Neurosci. 1:11-38.

[32] D. Hansel, G. Mato, and C. Meunier. Synchrony in excitatory neural networks. Neural Comp. **7**, 307-337 (1995).

[33] Hanson FE. Comparative studies of firefly pacemakers. Fed Proc. 1978 Jun;37(8):2158-64.

[34] Hodgkin, AL (1948) The local changes associated with repetitive action in a non-medulated axon. J. Physiol (London) 107: 165-181

[35] Izhikevich E.M. (2000) Neural Excitability, Spiking, and Bursting. International Journal of Bifurcation and Chaos. 10:1171-1266.

[36] Izhikevich E.M. (2003) Simple Model of Spiking Neurons IEEE Transactions on Neural Networks, in press

[37] Kopell,-N.; Ermentrout,-G.-B., Symmetry and phaselocking in chains of weakly coupled oscillators. Comm.-Pure-Appl.-Math. 39 (1986), no. 5, 623–660.

[38] Kopell,-N.; Ermentrout,-G.-B., Phase transitions and other phenomena in chains of coupled oscillators. 1990 SIAM-J.-Appl.-Math. 50 (1990), no. 4, 1014–1052.

[39] N. Kopell and G.B. Ermentrout. "Mechanisms of phaselocking and frequency control in pairs of coupled neural oscillators", for Handbook on Dynamical Systems, vol. 2: Toward applications. Ed. B. Fiedler, Elsevier, pp 3-5. (2002)

[40] Kopell N, Ermentrout GB, Whittington MA, Traub RD. Gamma rhythms and beta rhythms have different synchronization properties. Proc Natl Acad Sci U S A. 2000 Feb 15;97(4):1867-72.

[41] Y. Kuznetsov, Elements of Applied Bifurcation Theory, Springer, NY, 2000, page 83.

[42] Lam YW, Cohen LB, Wachowiak M, Zochowski MR. Odors elicit three different oscillations in the turtle olfactory bulb. J Neurosci. 2000 Jan 15;20(2):749-62.

[43] P.E. Latham, B.J. Richmond, P.G. Nelson, and S. Nirenberg. Intrinsic dynamics in neuronal networks. I. Theory. J. Neurophysiol. 83(2):808-827 (2000).

[44] Lindner, B. and Longtin, A. Neural Computation, (in press) 2003

[45] E. Marder and R.L. Calabrese, 1996, Principles of rhythmic motor pattern generation, Physiological Reviews, 687-717.

[46] Murray, J.D. Mathematical Biology, Springer NY 1989

[47] Nenadic Z, Ghosh BK, Ulinski Propagating waves in visual cortex: a large-scale model of turtle visual cortex. J Comput Neurosci. 2003 Mar-Apr;14(2):161-84.

[48] Osan R, Rubin J, Ermentrout B Regular traveling waves in a one-dimensional network of theta neurons SIAM J APPL MATH 62 (4): 1197-1221 APR 22 2002

[49] Paullet, J.E and Ermentrout, G.B. Stable rotating waves in two-dimensional discrete active media. SIAM-J.-Appl.-Math. 54 (1994), no. 6, 1720–1744.

[50] Pinto, D.J. and Ermentrout, G.B. 2001a, Spatially Structured Activity in Synaptically Coupled Neuronal Networks: II. Lateral Inhibition and Standing Pulses, SIAM J. Appl Math. 62(1):226–243

[51] Pinto, D.J. and Ermentrout, G.B. 2001b, Spatially Structured Activity in Synaptically Coupled Neuronal Networks: I. Traveling Fronts and Pulses SIAM J. Appl Math. 62(1):206–225

[52] Ren, LW and Ermentrout, G.B. Monotonicity of phaselocked solutions in chains and arrays of nearest-neighbor coupled oscillators. SIAM-J.-Math.-Anal. 29 (1998), no. 1, 208–234

[53] Reyes AD, Fetz EE, (1993a) Effects of transient depolarizing potentials on the firing rate of cat neocortical neurons. J Neurophysiol 1993 May;69(5):1673-83

[54] Rinzel-J; Ermentrout-B, Analysis of neural excitability and oscillations, In "Methods in Neuronal Modelling: From synapses to Networks", C. Koch and I. Segev, eds. 1989, MIT Press (revised 1998).

[55] Jonathan Rubin and David Terman, "Geometric Singular Perturbation Analysis of Neuronal Dynamics," in B. Fiedler, editor, Handbook of Dynamical Systems, vol. 3: Toward Applications, Elsevier, 2002.

[56] Schoner G, Jiang WY, Kelso JA. A synergetic theory of quadrupedal gaits and gait transitions. J Theor Biol. 1990 Feb 9;142(3):359-91.

[57] W. Singer, 1993, Synchronization of cortical activity and its putative role in information processing and learning, Ann Rev. Physiol, 55:349-374.

[58] M. Stopfer, S. Bhagavan, B.H. Smith, and G. Laurent, 1997, Impaired odour discrimination on desynchronization of odour-encoding neural assemblies, Nature 390:70-74.

[59] Traub RD, Jefferys JG, Whittington MA. Simulation of gamma rhythms in networks of interneurons and pyramidal cells. J Comput Neurosci. 1997 Apr;4(2):141-50.

[60] Traub RD, Whittington MA, Stanford IM, Jefferys JG. A mechanism for generation of long-range synchronous fast oscillations in the cortex. Nature. 1996 Oct 17;383(6601):621-4.

[61] Van Vreeswijk C, Abbott L, and Ermentrout B. When inhibition not excitation synchronizes neural firing. J Comput Neurosci. 1994 Dec; 1(4):313-21.

[62] Wang X.-J. (1999a) Synaptic basis of cortical persistent activity: the importance of NMDA receptors to working memory. J. Neurosci. 19, 9587-9603.

[63] White JA, Chow CC, Ritt J, Soto-Trevino C, and Kopell N. Synchronization and oscillatory dynamics in heterogeneous, mutually inhibited neurons. J. Comp. Neurosci. 5, 5-16 (1998).

[64] Winfree, A.T. Biological rhythms and the behavior of populations of coupled oscillators, J. Theoret. Biol. 16:15-42, 1967.